A 6Gbps Transmitter with ISI and Reflection Cancellation

by

Ricky Yuen

A thesis submitted in conformity with the requirements
for the degree of Master of Applied Science
Graduate Department of Electrical and Computer Engineering
University of Toronto

A 6Gbps Transmitter with
ISI and Reflection Cancellation

Ricky Yuen

Master of Applied Science, 2005
Graduate Department of Electrical and Computer Engineering
University of Toronto

Abstract

This thesis presents the design and implementation of a high-speed chip-to-chip transmitter with Intersymbol Interference (ISI)-cancellation circuitry and reflection-cancellation circuitry. The transmitter has a 2-way interleaving architecture with an aggregate data rate of 6Gbps. To cancel ISI, the transmitter uses a 3-tap pre-emphasis driver. As for the reflection-cancellation circuitry, the transmitter uses an 8-tap reflection canceller with one Unit Interval (UI) resolution. The 8 continuous taps can be delayed from 0 to 126 unit intervals to match the timing of the reflections. A testchip of the transmitter is designed in Fujitsu's $0.11\mu m$ CMOS technology to demonstrate our reflection-cancellation technique. The testchip includes a $3GHz$ Phase Locked Loop (PLL) to serve as a clock generator for the transmitter testchip.

Acknowledgements

Contents

List of Figures

List of Tables

List of Acronyms

BER Bit Error Rate

BERT Bit Error Rate Tester

CMOS Complementary Metal Oxide Silicon

dB Decibel

DFE Decision Feedback Equalizer

FLA Fujitsu Laboratories of America

FSM Finite State Machine

GHz Giga Hertz

LC Inductor and Capacitor

IEEE Institute of Electrical and Electronics Engineers

IC Integrated Circuit

ISI Intersymbol Interference

JTAG Joint Test Action Group

LSB Least Significant Bit

MHz Mega Hertz

MOSFET Metal Oxide Semiconductor Field Effect Transistor

MSB Most Significant Bit

NMOS Negative-Channel Metal Oxide Semiconductor

PCB Printed Circuit Board

PRBS Pseudo Random Bit Sequence

PMOS Positive-Channel Metal Oxide Semiconductor

PLL Phase Locked Loop

RMS Root Mean Square

UI Unit Interval

VCO Voltage Controlled Oscillator

1 Introduction

1.1 Motivation

The need to quickly transfer large amount of data between chips on Printed Circuit Boards (PCBs) has accelerated the research of high-speed signaling. New circuit techniques have been developed to allow faster data transmission [FMWK97], to have more accurate data recovery [SR01], and to obtain better signal quality [FMWK97] [Son96] [KFM02]. With these circuit techniques, transceivers are able to transmit several gigabits of data per second per pin over PCB traces [FMWK97] [TTM+03].

The increase in signaling speed over PCB traces introduces transmission line effects on the signal. Examples of transmission line effects include skin effect and reflection. Skin effect of a conductor, such as a PCB trace, causes high frequency components of the travelling signal to concentrate at the periphery of the conductor and leads to an increase in its resistance. Skin effect is the dominant cause of the frequency-dependent attenuation of PCB traces [HHM00], and manifests itself as intersymbol interference (ISI). ISI causes the energy of a single bit to spread to adjacent bits causing interference. Reflections occur when signals experience impedance mismatches along the channel. These reflections, if they travel back to the receiver, interfere with the received signal. Signal interference caused by ISI and reflection leads to higher bit error rate (BER) and limits data transmission speed.

Channels in backplane systems could have many impedance mismatches that cause reflections. A backplane is a type of system that has multiple line cards communicating over a common channel. The chips on the line cards are connected in a bus topology through the use of connectors, vias, and PCB traces [HHM00]. In addition, the chips are usually packaged before they are soldered on the line cards. Thus, the channel for chip-to-chip signaling on the backplane includes not only the PCB trace that causes ISI, but also the connectors, vias, and chip packagings that cause reflections.

Reflections and ISI affect the received signal on backplanes and lead to detection er-

rors. The transceiver developed by Zerbe et al. [ZWS$^+$03] uses a pre-emphasis scheme to equalize ISI and a Decision Feedback Equalizer (DFE) to cancel reflections. Pre-emphasis is a method implemented in the transmitter to equalize ISI by amplifying the high frequency components of the transmitted signal, in anticipation of the frequency dependent loss of the channel. DFE is a method implemented in the receiver to compensate for the loss of the received signal prior to signal detection. However, a DFE has a more complicated implementation compared to pre-emphasis. This is because a DFE deals with both the analog received signal and the digital recovered signal while a pre-emphasis driver only deals with the digital data bits.

By extending the idea of pre-emphasis, we propose implementing the reflection cancellation at the transmitter. Instead of canceling reflections at the receiver, the transmitter is programmed to send out reflection-cancellation signals such that the sum of the reflection signal and the cancellation signal is zero. The benefits of cancelling reflections at the transmitter are increased effectiveness, accuracy, and ease of implementation. By canceling the reflections before they travel back to the receiver, this technique eliminates the occurrences of multiple reflections that further interfere with the received signal.

1.2 Objective

The objective of this research is to develop a transmitter with reflection cancellation and ISI cancellation capability for high-speed chip-to-chip signaling. A $3GHz$ PLL is to be designed as the clock generator for the transmitter. The transmitter has a targeted data rate of 6Gbps. A testchip of the transmitter will be implemented with Fujitsu Laboratories of America (FLA) $0.11\mu m$ CMOS process.

1.3 Organization of the Thesis

The subsequent chapters of the thesis are organized as follows. Chapter 2 covers the background material on high-speed signaling, including ISI for long and lossy channels as well as signal reflections due to impedance mismatches. Chapter 2 also discusses previous approaches for compensating ISI. Chapter 3 presents our approach to equalizing the signal reflection at the transmitter. This chapter also provides details of the transmitter circuits including the transmitter digital block, the transmitter front-end, and a $3GHz$

PLL designed as a clock generator for the transmitter. Chapter 4 shows the simulation results for both the transmitter and the PLL. Simulations include received signal eye diagrams showing the improvments in the eye opening, with the reflection-cancellation drivers enabled. Finally, chapter 5 concludes the thesis by summarizing the contributions of this research.

2 Background: High-Speed Signaling

A simplified architecture of a chip-to-chip signaling system is shown in Figure 2.1. The system contains a transmitter, a channel for data transmission, and a receiver. The transmitter is the chip that sends data onto the channel. The channel is the medium, such as a PCB trace, on which electrical signals travel. The receiver is the chip that recovers the original data from the received signal. The performance of chip-to-chip signal systems depends on all three components since they are interrelated [Buc03].
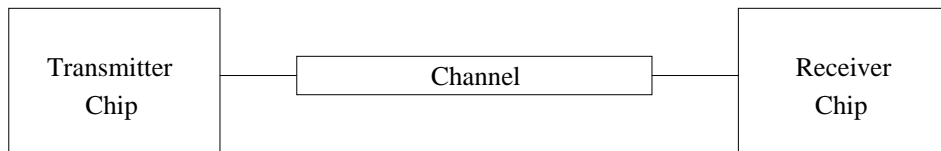
Figure 2.1: Simplified chip-to-chip signaling system.

2.1 Lossy Transmission Line and Intersymbol Interference

Channels with flat frequency responses do not distort signals they carry. However, practical PCB channels in chip-to-chip signaling systems suffer from skin effect, which causes frequency-dependent attenuation of the signals [HHM00]. Figure 2.2 shows the frequency response of a typical 50Ω PCB channel. The channel is a $50cm$ PCB trace modelled with W-element in Hspice as shown in Figure 2.3. Simulation results show that the channel exhibits severe attenuation for signal frequency components beyond $1GHz$. The results also show that the channel acts as a low-pass filter to the signals it carries.

In the time-domain, frequency-dependent attenuation of the channel manifests itself as intersymbol interference (ISI). ISI causes attenuation of the transmitted signal and spreads the energy of the transmitted signal into adjacent bits causing interference. The
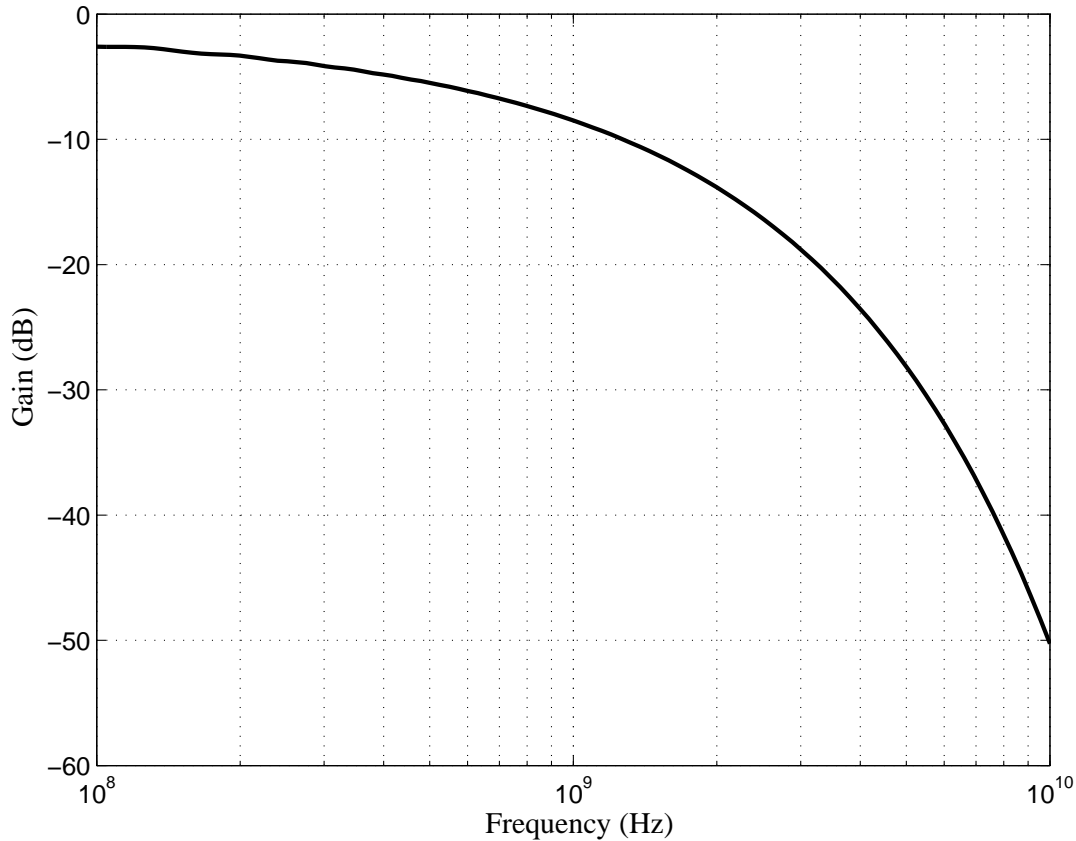
Figure 2.2: Channel frequency response of a $50cm$ PCB trace.

effect of ISI in time-domain is illustrated in Figure 2.4. The signal in Figure 2.4 (a) is the transmitted pulse with $1ns$ duration. The pulse arrives at the receiver at $7ns$ and is being attenuated to $160mV$ from $200mV$ as shown in Figure 2.4 (b). ISI also causes a $20mV$ residue to spread to and interfere with the next bit.

The effect of ISI on the received signal during high-speed data transmission is shown in Figure 2.5. The data is transmitted at 6Gbps with an amplitude of $200mV$. After passing through the channel, the received signal is significantly attenuated by ISI. Some bits in the received signal barely cross the threshold voltage of $100mV$, making it difficult for the receiver to recover the original data. Thus, ISI causes interference in the received signal and leads to detection errors.
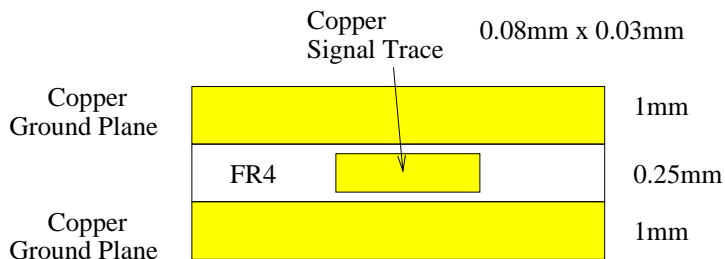
Figure 2.3: Cross sectional view of a PCB W-element model.

2.2 Equalization Techniques

In general, there are two methods to cancel the effect of ISI. First, a pre-emphasis driver can be implemented in the transmitter to pre-distort the transmitted signal, in anticipation of the frequency-dependent loss of the channel. Second, a post-equalizer can be implemented in the receiver to compensate for the channel loss before the receiver attempts to recover the original data. The ideas behind pre-emphasis equalization and post-equalization are discussed in the following.

2.2.1 Pre-Emphasis Equalization

Pre-emphasis equalization is implemented in the transmitter to cancel the effect of ISI. The idea behind pre-emphasis is illustrated in Figure 2.6. PCB channels have low-pass frequency responses due to skin effect. To cancel the effect of ISI, a block with a high-pass frequency response is inserted in the transmitter. Thus, the complete channel, which includes the pre-emphasis block and the PCB channel, has a flat frequency response.

The high-pass frequency response of the pre-emphasis block is created by attenuating the low frequency components of the transmitted signal [DP97]. In the time-domain, the result of attenuating the low frequency component of the transmitted signal makes the signal amplitude after transition larger than the signal amplitude without transition as shown in Figure 2.7 (a). For example, the amplitude of the transmitted signal after transition is $200mV$, whereas signal amplitude without transition is $180mV$. By emphasizing on the signal transitions, the received signal is able to remove the interference caused by ISI as shown in Figure 2.7 (b).

One way to create the pre-emphasized signal is by using current-mode signaling as shown in Figure 2.8. The $7.6mA$ data driver is connected together with the $400\mu A$
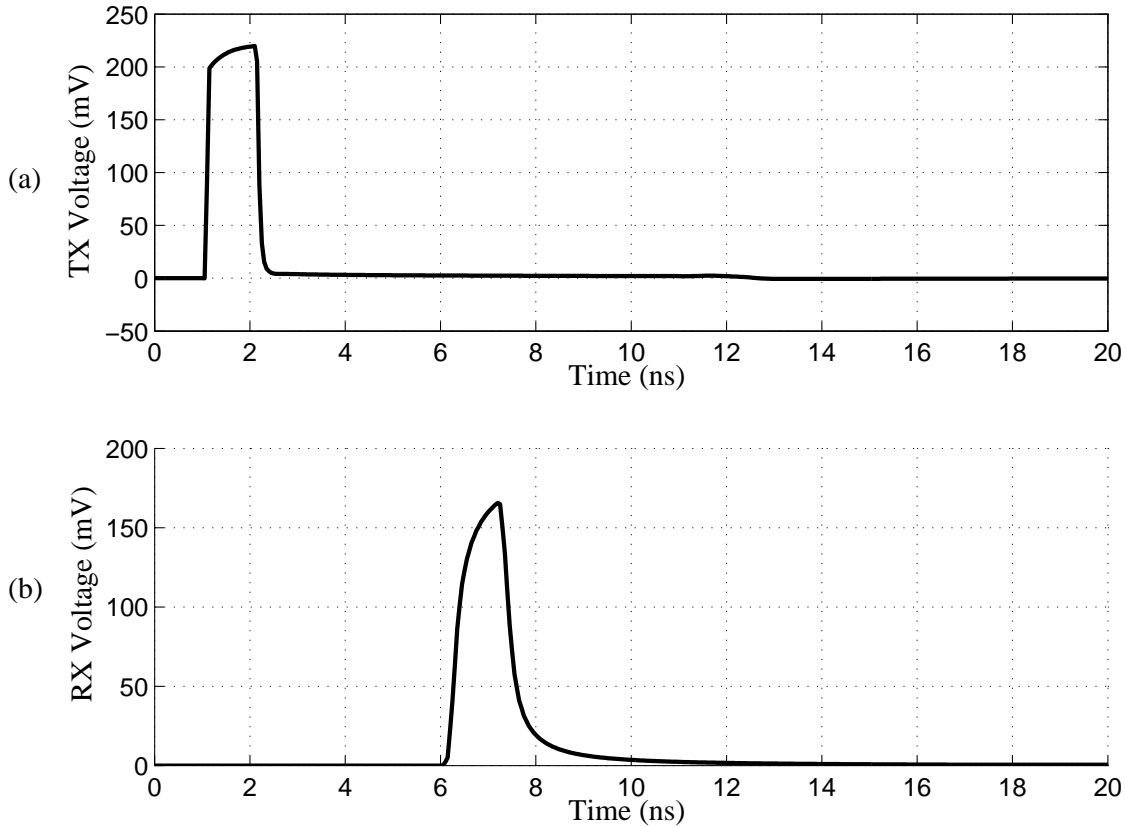
Figure 2.4: ISI in a $50cm$ PCB trace. (a) Channel input transient response. (b) Channel output transient response.

pre-emphasis driver at the output nodes, *txout* and *txoutx*. *dn* and *dnx* are data inputs, and $d(n-1)$ and $d(n-1)x$ are data inputs delayed by one UI.

To illustrate how the pre-emphasis driver functions, the transmitted data is assumed to be equal to $d_n =$ [-1, 1, -1, -1]. The data driver produces $190mV$ of output swing and the pre-emphasis driver produces $10mV$ of output swing as shown in Figure 2.9. The polarity of the 1UI delayed data to the pre-emphasis driver is flipped to emphasize the signal transitions. The output of the pre-emphasis driver is the inverted and 1UI delayed version of the output of the data driver. The pre-emphasized signal is created by current summing the output of the data driver and the pre-emphasis driver.

Recently, a 5Gbps transmitter with pre-emphasis is designed by Lin as shown in Figure 2.10 [LWJ03]. The main driver has $10.5mA$ of current which produces $250mV$ output swing. There are two pre-emphasis drivers: $Tap1$ uses the 1UI delayed data and $Tap2$

7
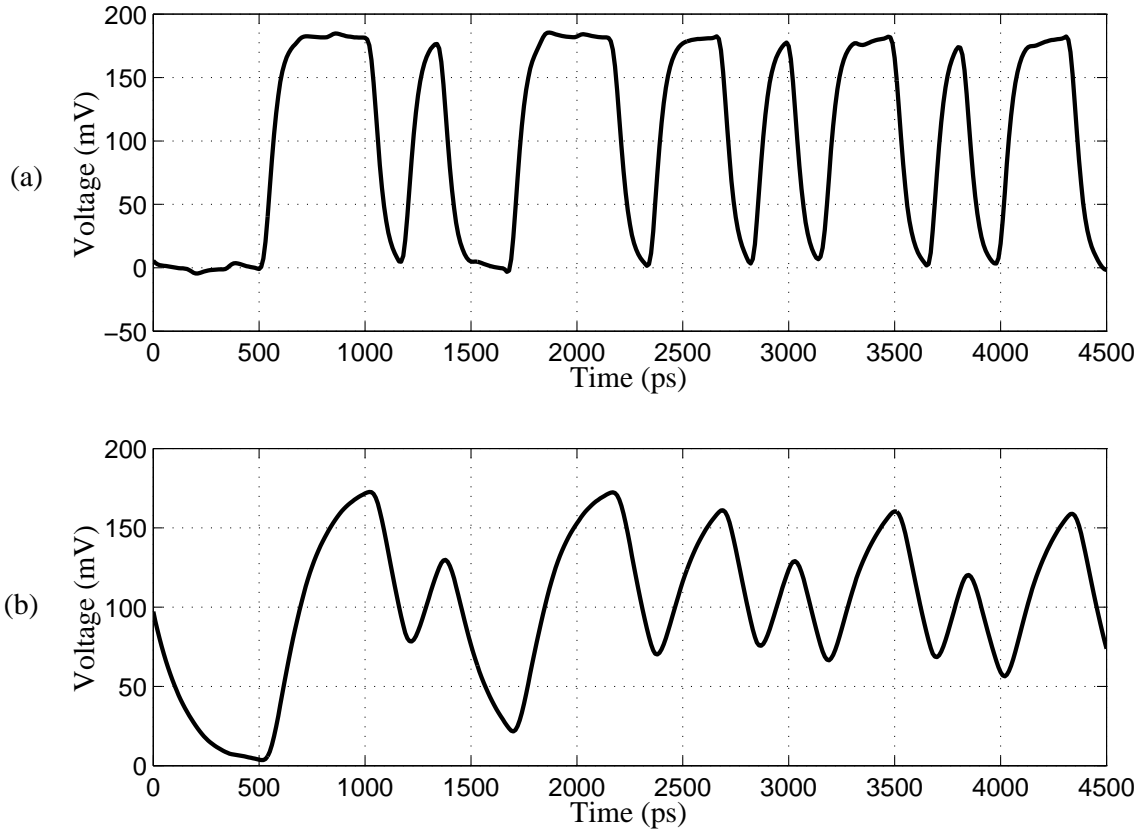
Figure 2.5: Data transmission affected by ISI. (a) Transmitted signal. (b) Received signal.
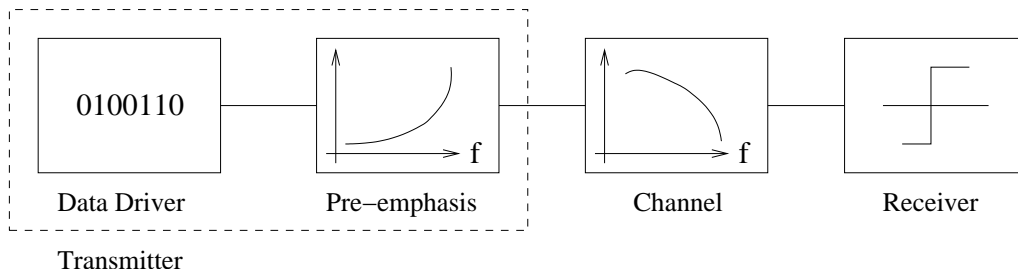
Figure 2.6: The idea behind pre-emphasis equalization.

uses the 2UI delayed data. The current in $Tap1$ is controlled by a 7-bit digital input and the current in $Tap2$ is controlled by a 3-bit digital input. With this architecture, the transmitter is able to transmit data at 5Gbps over a $15m$ coaxial cable.
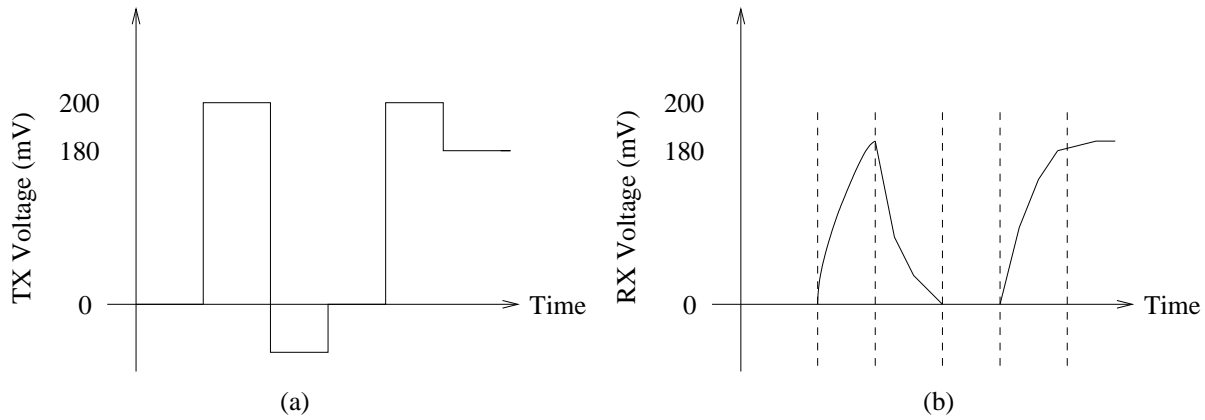
Figure 2.7: Data transmission with pre-emphasis. (a) Transmitted signal. (b) Received signal.
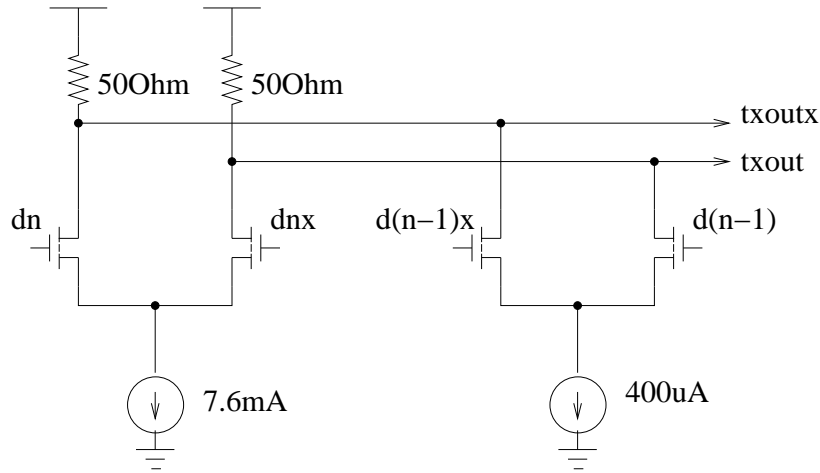
Figure 2.8: Pre-emphasis circuit implementation.

2.2.2 Post-Equalization

Post-equalization is implemented in the receiver to cancel ISI. The purpose of a post-equalizer is to create a channel with a flat frequency response between the transmitter and the receiver. Unlike pre-emphasis equalization, the post-equalizer allows the ISI to corrupt the signal during transmission but cancels the ISI before the receiver attempts to recover the original data. The idea behind post-equalization is illustrated in Figure 2.11.

Two main implementations of post-equalization are: the feed-forward equalizer and
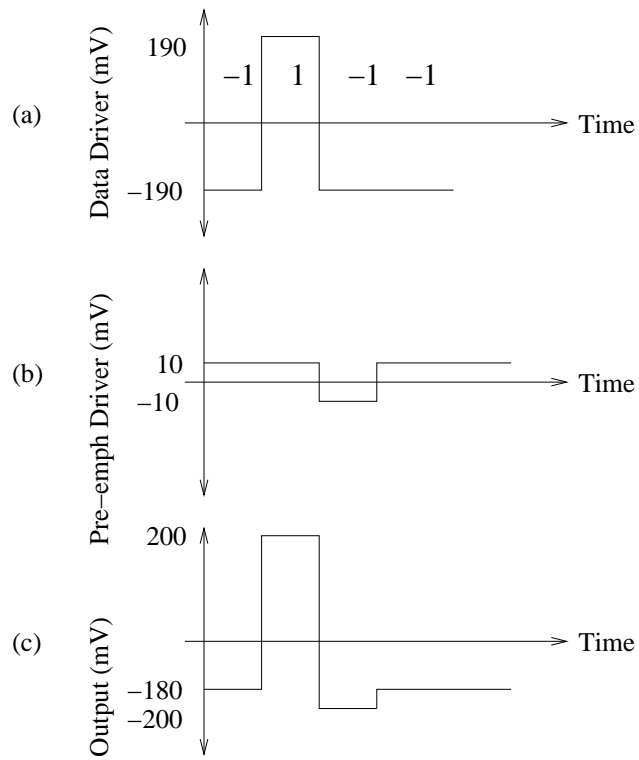
Figure 2.9: The generation of the pre-emphasis waveform. (a) Signal from data driver. (b) Signal from pre-emphasis driver. (c) Signal at the output node.
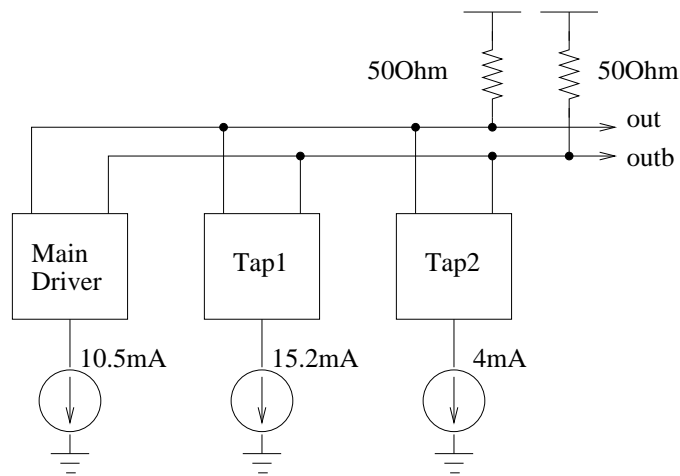
Figure 2.10: The transmitter implemented by Lin [LWJ03].
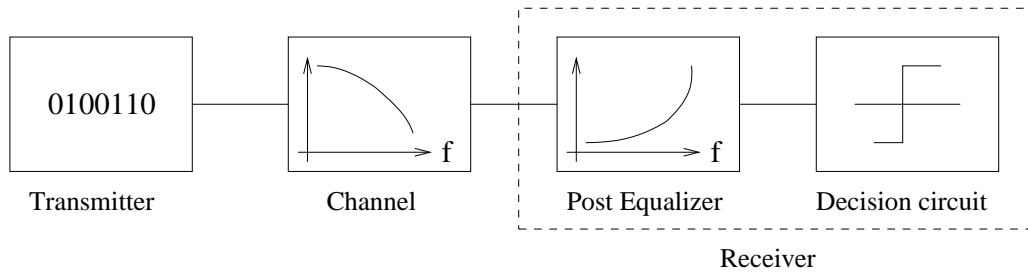
Figure 2.11: The idea behind post-equalization.

the Decision Feedback Equalizer (DFE). The feed-forward equalizer samples the received signal, and subtracts from it a fraction of the previous sample. The amount of subtraction depends on the ISI in the current sample. Figure 2.12 shows the block diagram of a feed-forward equalizer where the depth of ISI is one. This means ISI only cause interference to one adjacent bit. Extra feed forward paths are required to cancel ISI with depth higher than one.
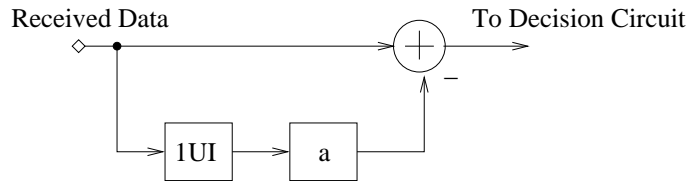
Figure 2.12: The idea behind feed-forward equalizer.

The idea behind a DFE is similar to a feed-forward equalizer. Instead of subtracting a fraction of the previous sample from the current sample of the received signal, a DFE subtracts a scaled version of the recovered data from the current sample of the received signal. Figure 2.13 shows the block diagram of a DFE where the depth of ISI is one. The received signal r is subtracted by a correction signal given by $a \times d(n-1)$, where $d(n-1)$ is the previous recovered data and a is the scale factor. The result of the subtraction s, the ISI-free received signal, enters the decision circuit to recover the original data.

Figure 2.14 illustrates the ISI subtraction in the DFE. The received signal r shown in Figure 2.14 (a) has ISI equal to c. To cancel the ISI, it is necessary to subtract c from the received signal at time $t(n+1)$. The correction signal is the scaled version of the recovered data as shown in Figure 2.14 (b). The correction signal is subtracted from the received signal r to become the ISI-free signal s as shown in Figure 2.14 (c).

11
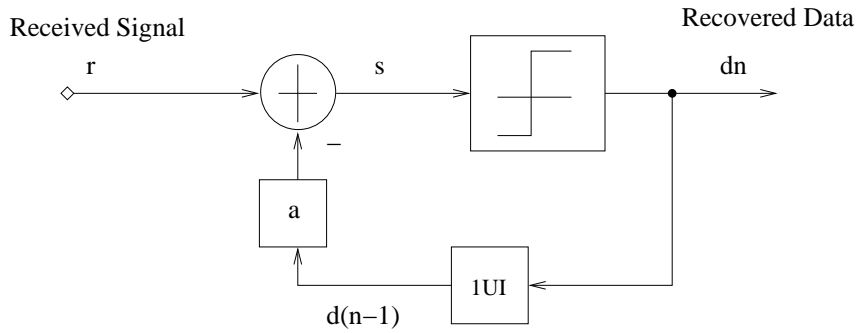
Figure 2.13: DFE block diagram.
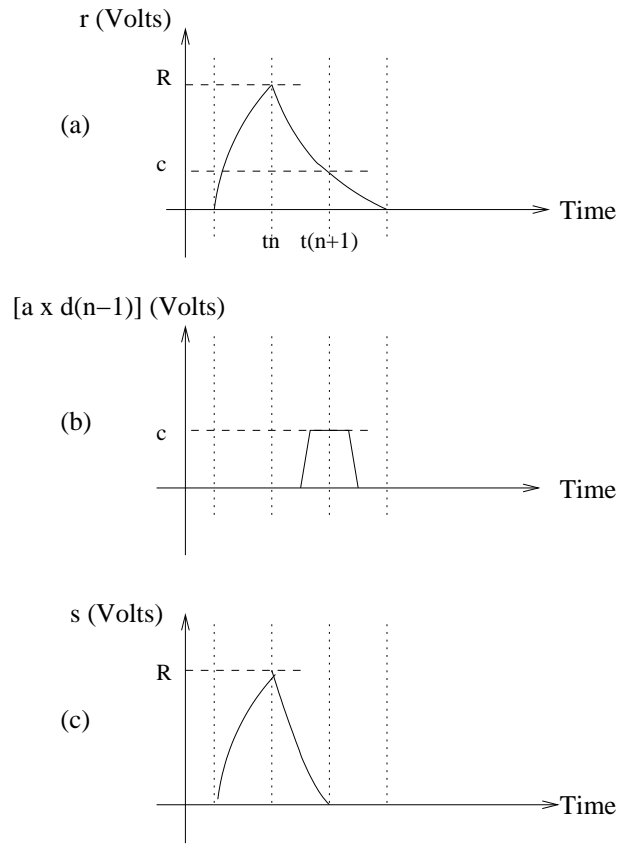
Figure 2.14: The DFE ISI correction process. (a) The received signal. (b) The feedback signal. (c) The ISI-free signal ready for detection.

2.3 Reflections

Channels in backplane systems have many impedance discontinuities that cause reflections to occur. Reflections, similar to ISI, interfere with the received signal and lead to

12

detection errors. Practically, reflections are unavoidable since any impedance mismatch along the channel lead to reflections. Examples of impedance mismatches in backplane systems include PCB vias, connectors, bondwires, and termination resistors.

Reflections can be classified into three main types: resistive, capacitive, and inductive [HHM00]. Resistive reflection is the simplest to understand as the reflection is only an attenutated version of the original signal. Examples of impedance mismatches that cause resistive reflections include PCB vias and termination resistors. Capacitors and inductors are time-dependent elements and generate reflections that look different from the original signal. Connectors, for example, cause capacitive reflections while bondwires and PCB vias cause inductive reflections in backplane systems.

2.3.1 Resistive Reflection

Resistive reflections occur when characteristic impedances change along the channel. The change of impedance can occur at the termination or at the junction between two PCB traces with two different characteristic impedances. Figure 2.15 illustrates the effect of resistive reflection. The channel with characteristic impedance Z_o is terminated at both the transmitter and receiver sides by resistors r_{tx} and r_{rx} respectively. If $r_{tx} = r_{rx} = Z_o$, the channel is perfectly terminated and there is no reflection.
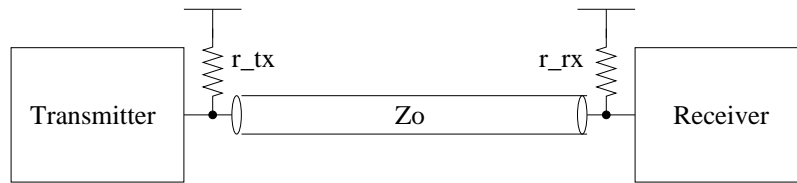
Figure 2.15: Resistive reflection from termination mismatches.

To show resistive reflections, it is assumed that $Z_o = 50\Omega$ and $r_{tx} = r_{rx} = 55\Omega$. Figure 2.16 is a lattice diagram showing the multiple reflections that happen at the transmitter and receiver sides. The reflection coefficient ρ represents the amount of the original signal that gets reflected when the original signal comes across the impedance mismatch. At the transmitter side, the reflection coefficient is equal to (2.1).

$$\rho_{tx} = \frac{r_{tx} - Z_o}{r_{tx} + Z_o} \tag{2.1}$$

At the receiver side, the reflection coefficient is equal to (2.2).

$$\rho_{rx} = \frac{r_{rx} - Z_o}{r_{rx} + Z_o} \qquad (2.2)$$

In this example, $\rho_{tx} = \rho_{rx} = 0.048$, which means that only 4.8% of the original signal gets reflected back to the source. The channel has an attenuation factor of $\sigma = 0.9$, which means only 90% of the transmitted signal appears at the output of the channel. At time $t = 0$, the transmitter sends out a $1V$ square pulse to the receiver. The $1V$ pulse is voltage divided by the termination resistor and the characteristic impedance of the channel, which results in only $476mV$ appearing on the channel. After one channel delay (1D), the attenuated signal appears at the receiver with an amplitude of $428mV$. Since 4.8% of the original signal gets reflected, $21mV$ travels back to the transmitter and arrives at the transmitter at time 2D with an amplitude of $19mV$. The signal is reflected again and the reflection travels back to the receiver causing interference to the received signal at that time. This example shows multiple resistive reflections that are caused by imperfect resistor terminations.
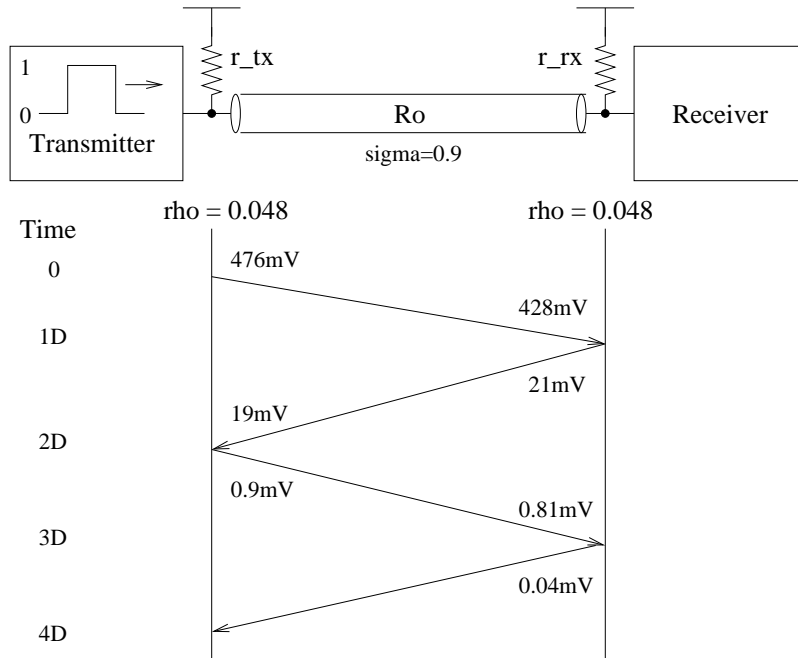
Figure 2.16: Lattice diagram showing multiple resistive reflections.

2.3.2 Capacitive Reflection

Capacitive reflections occur when signals come across any capacitive component along the channel. Major capacitive reflections happen at connectors or bonding pads that act as large capacitances to the signal. Figure 2.17 shows a connector, modelled by a capacitor, located on the channel. The channel is assumed to be terminated properly at both the transmitter and receiver ends.
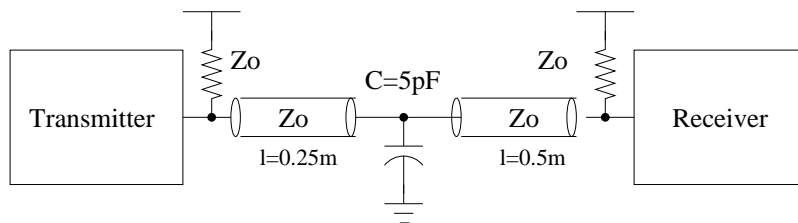
Figure 2.17: Capacitive reflection from connectors.

When capacitors are excited by a step response, they will initially act as short circuits and then charge up with a time constant of $\tau = CZ_o$ [HHM00]. After they are charged up, they will look like open circuits. The reflection coefficient ρ for a short circuit is equal to -1 and for an open circuit is $+1$. Thus, signals reflect negatively at first and reflect positively after the capacitor is charged up.

Figure 2.18 illustrates a pulse response simulation with the channel in Figure 2.17. The $200mV$ square pulse is sent to the channel and the capacitive reflection comes back to the transmitter at $4.5ns$. The shape of the reflection is different than the original pulse.

The capacitor acts as a short circuit to the positive edge of the pulse. Since it experiences a reflection coefficient of -1, it reflects negatively back to the transmitter. The reflection is shown from the first part of the reflection in Figure 2.18 as it dips down towards the negative direction. After the capacitor is fully charged up, the reflection coefficient changes back to $+1$ and the reflection goes back to zero. The opposite scenerio is true for the negative edge of the square pulse. The reflection rises in the positive direction and goes back to zero when the reflection coefficient changes to $+1$.

The amplitude of the reflection is dependent on the charge up time of the capacitor. The charge up time of the capacitor is dictated by the time constant, $\tau = CZ_o$. The time duration between the start of the reflection to the peak of the reflection is the charge up
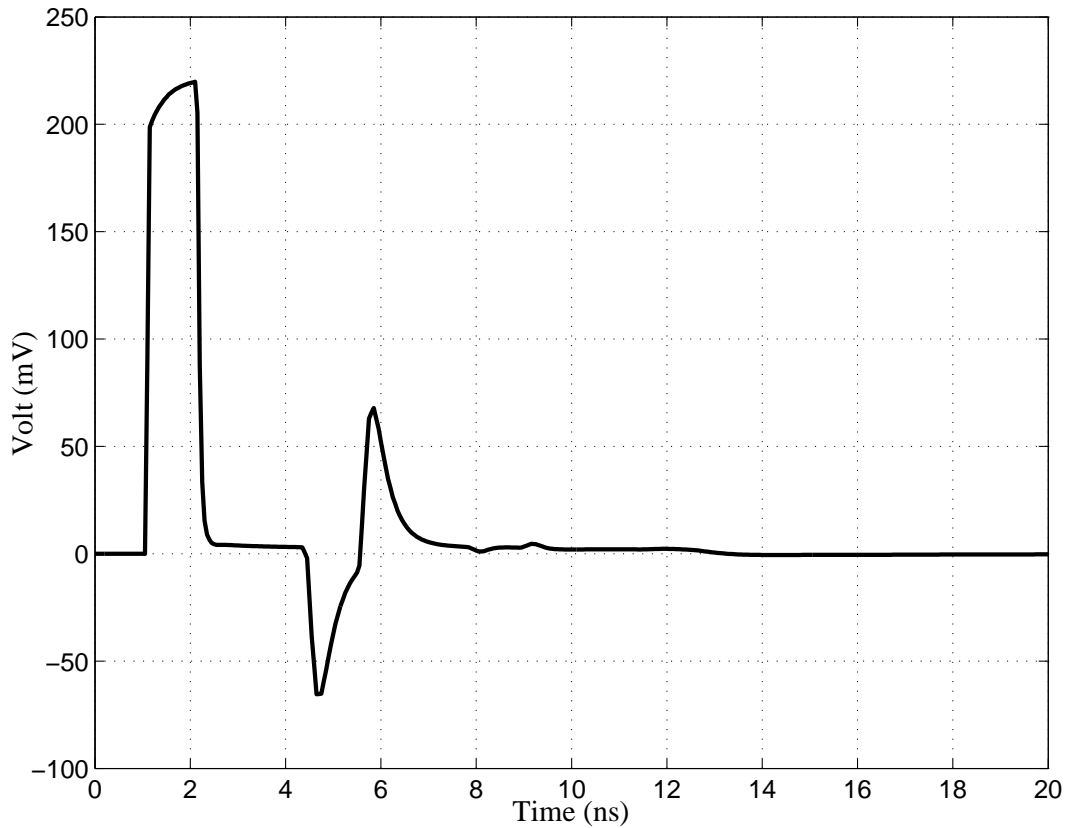
Figure 2.18: Simulation of capacitive reflection along the channel.

time of the capacitor. Thus, larger capacitors result in larger reflections.

2.3.3 Inductive Reflection

Inductive reflections look similar to capacitive reflections. However, inductors act as open circuits initially and eventually become short circuits. When signals come across inductors, they initially experience a reflection coefficient of $+1$ and the coefficient will gradually change to -1. Figure 2.19 shows a channel with a bondwire modelled by an inductor.

The pulse response simulation with the channel in Figure 2.19 is shown in Figure 2.20. The transmitter sends a $200mV$ pulse to the receiver and the inductive reflection comes back to the transmitter at $4.5ns$. The positive edge of the transmitted pulse experiences a reflection coefficient of $+1$ and reflects positively back to the transmitter.
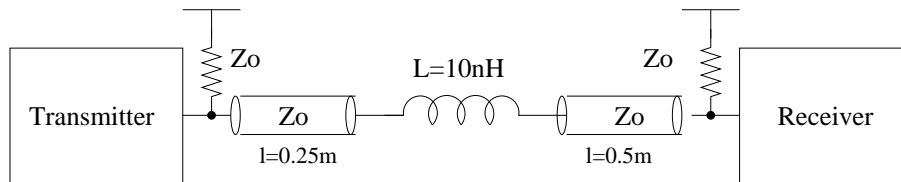
Figure 2.19: Inductive reflection along the channel.

As the inductor becomes a short circuit, the reflection coefficient changes to -1 and the reflection goes back to zero. The negative edge of the transmitted pulse repeats the reflection process when it reaches the inductor. The amplitude of the reflection is proportional to the time constant of the inductor, which is equal to $\tau = \frac{L}{Z_o}$. Thus, larger inductors results in larger reflections.
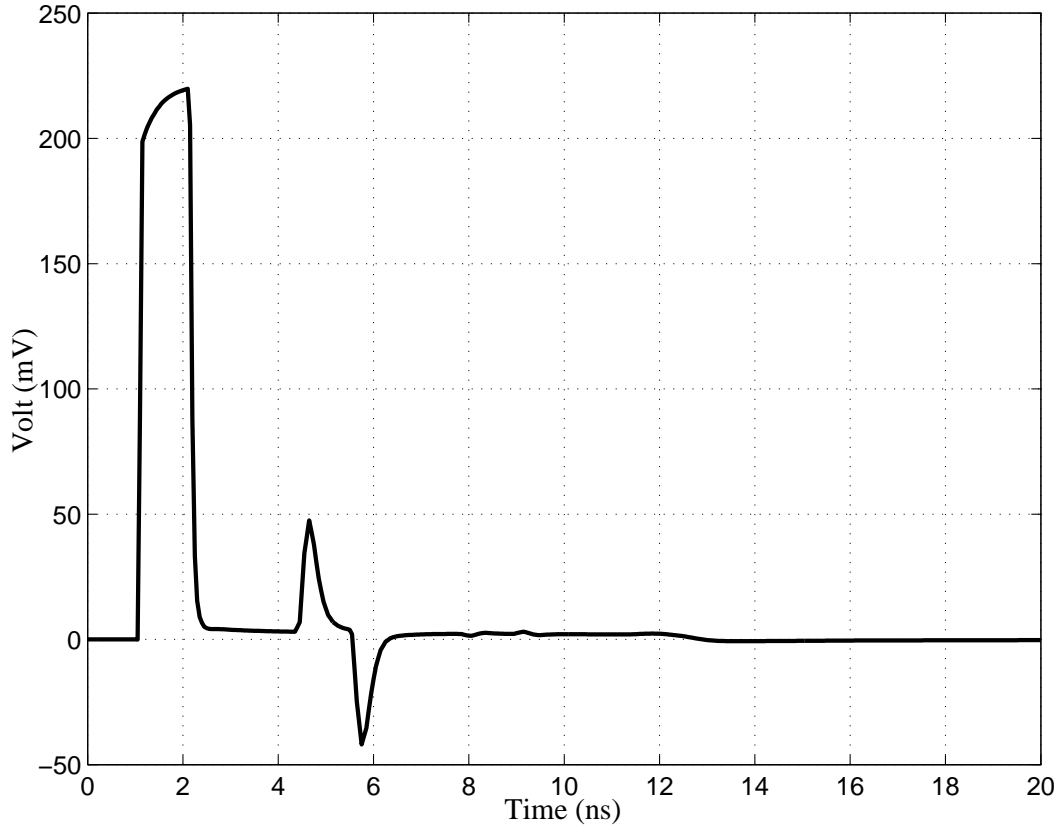
Figure 2.20: Simulation of inductive reflection along the channel.

2.4 Reflection Cancellation

Reflections, like ISI, interfere with the received signal and need to be cancelled. One way is to cancel the reflections at the transmitter. By sending out cancellation signals such that it is zero when summed with the reflection signal, the reflections are cancelled before they reach the receiver and eliminate the interference to the received signal. Since the reflections are cancelled before they travel back to the receiver, the occurrences of multiple reflections are eliminated. Chapter 3 discusses the architecture of a transmitter with reflection cancellation capability as well as the design and implementation of the transmitter.

2.5 System Simulation

System simulations are performed to estimate the amount of taps needed in the pre-emphasis equalization and the reflection canceller. The effect of ISI is most severe in long and lossy channels; whereas, the effect of reflection is worst in short channels with impedance discontinuities. Since the target application is backplane systems, line cards that are far apart experience ISI and those that are in close proximity experience reflection interference.

The channel model as shown in Figure 2.21 is used to estimate the number of pre-emphasis taps needed in a typical backplane system. The channel is a $1m$ PCB channel, which is modelled by a Hspice W-element. A $200mV$ 6Gbps pulse is sent to the channel to obtain the impulse response. The received signal is shown in Figure 2.22. The received signal experiences a 3-tap ISI of more than $10mV$. The ISI after three unit intervals is lowered than $10mV$ and will be assumed negligible.
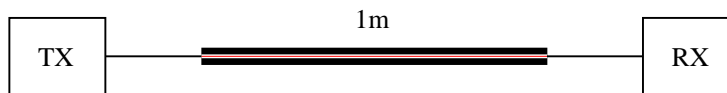
Figure 2.21: The $1m$ PCB channel used to determine the number of ISI taps needed.

For the reflection cancellation circuitry, the short channel with impedance disconti-nuities as shown in Figure 2.23 is used to determine the number of taps needed. The channel has three sections. The first and last sections, have a length of $5cm$, represent
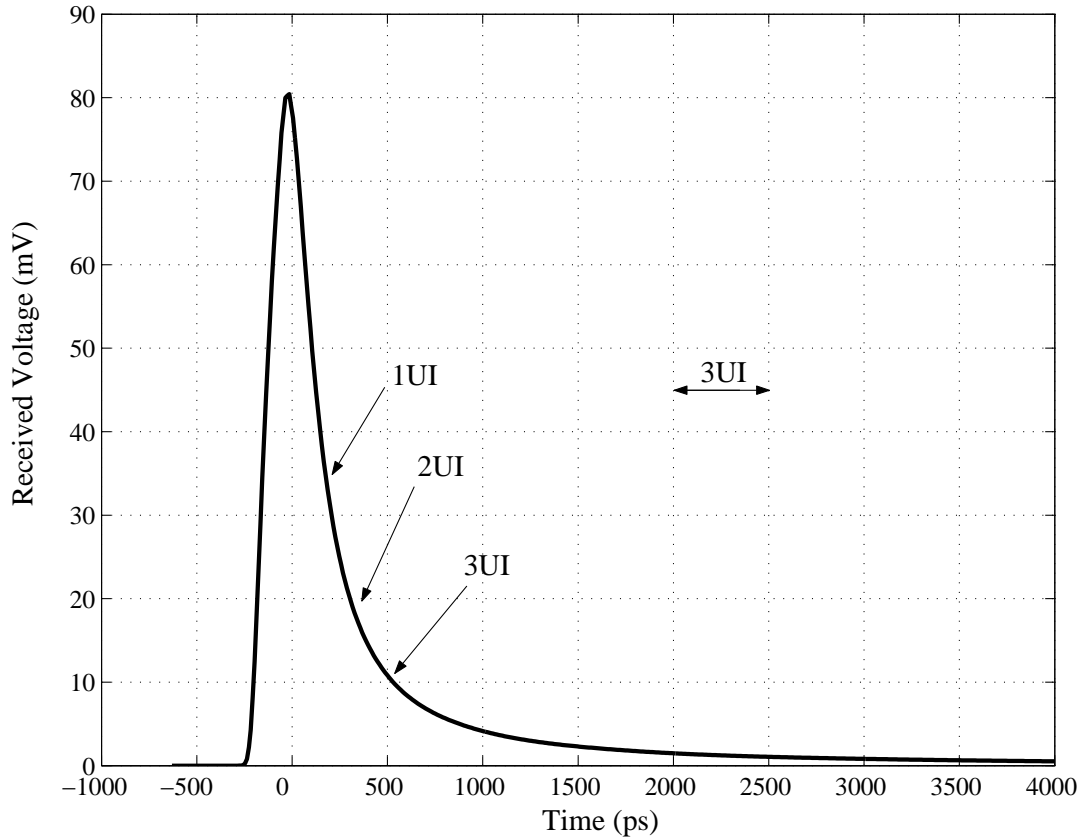
Figure 2.22: The impulse response of a $1m$ PCB channel.

the length of the PCB trace on the line card. The $8cm$ middle section represents the PCB channel on the backplane. The two $3pF$ capacitors represent the connectors used to connect the line cards to the backplane. A $200mV$ 6Gbps pulse is sent to the channel to obtain the impulse response as shown in Figure 2.24. The first reflection arrives at the receiver after $1ns$ for a duration of about six unit intervals. The secondary reflections caused by the first reflection are assumed to be negligible.
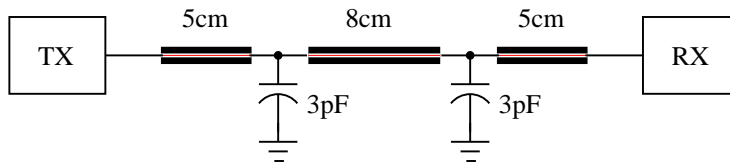
Figure 2.23: The PCB channel used to determine the number of reflection taps needed.
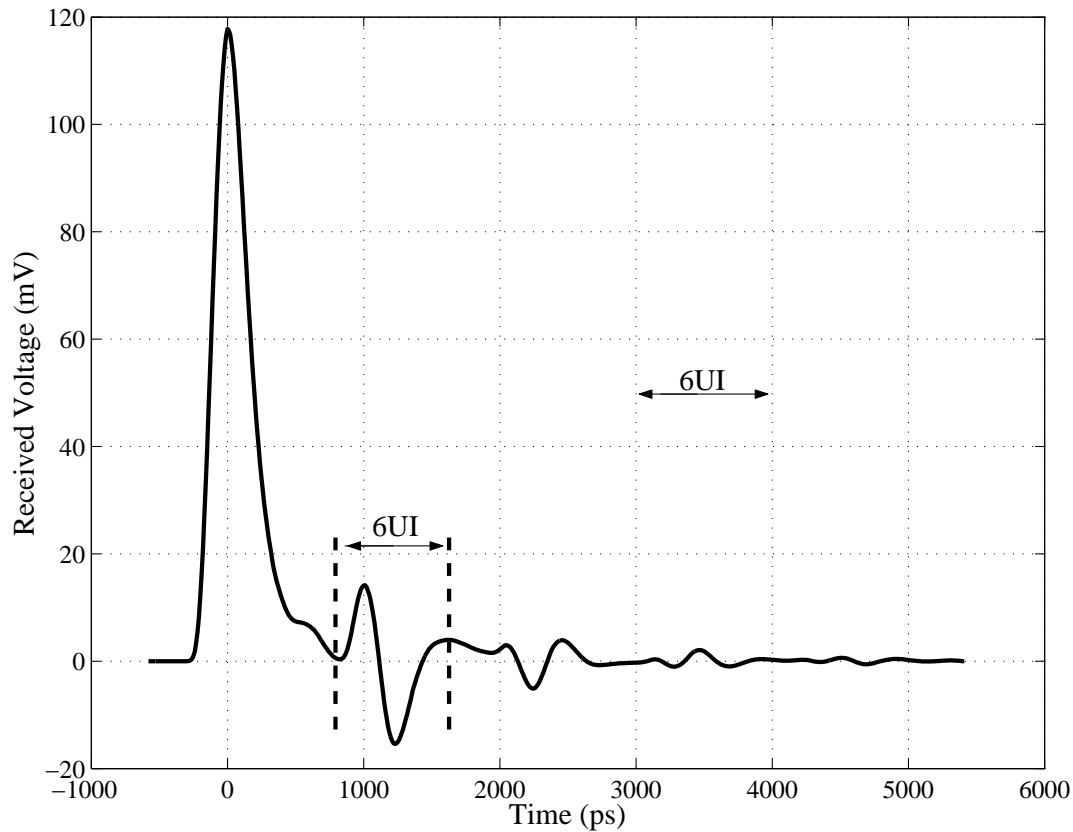
Figure 2.24: The impulse response of a $8cm$ PCB channel with connectors.

The above system simulations indicate that for typical backplane systems, 3-tap pre-emphasis equalization is adequate for $1m$ PCB channel at a data rate of 6Gbps. For the reflections that occur in the short channels, between two adjacent line cards, the number of taps should be more than six.

2.6 Summary

The frequency-dependent loss of PCB channels are caused by skin effect. Skin effect manifests itself as ISI in the time-domain and causes interference to the received signal. Methods for canceling ISI include implementing pre-emphasis equalization in the transmitter and implementing post-equalization in the receiver.

There are three different kinds of reflection: resistive, capacitive, and inductive. Resistive reflection is the simplest to understand as the reflections have the same shape as

the original signal. Capacitive and inductive reflections have different shapes due to the time-dependent nature of capacitors and inductors.

3 Transmitter Design

This chapter describes the design of a transmitter with ISI and reflection cancellation capabilities, targeted for backplane wireline channels. Figure 3.1 shows a system overview of the transmitter, consisting of a Phase Locked Loop (PLL), a digital block, high-speed multiplexors, a data driver, pre-emphasis drivers, and reflection-cancellation drivers. The transmitter uses a 2-way interleaving architecture, combining two half-rate data streams into one. This alleviates the speed constraints of a full-rate architecture in which digital circuits operate at the data rate. In terms of clock signals distribution, a 2-way interleaving architecture is superior to a 4-way interleaving architecture, as the former requires only two good-quality clock signals, while the latter requires four good-quality clock phases. Two data blocks, each operating on a different clock phase from the PLL, provide the half-rate transmitted data streams that are merged by the high-speed multiplexors. Finally, the data driver, the pre-emphasis drivers, and the reflection-cancellation drivers transmit the data to the channel. The pre-emphasis drivers are used to cancel the ISI using the technique described in Chapter 2. The technique used for reflection cancellation is discussed next.

3.1 Approach to Reflection-Cancellation

To cancel reflections, the reflection-cancellation drivers send out cancellation signals such that the sum of the reflection signal and the cancellation signal is zero. We describe our approach in reflection cancellation by means of signal waveforms at the transmitter output and receiver input illustrated in Figure 3.2. This example assumes that the transmitter and receiver terminations are different than the channel characteristic impedance. The transmitter sends out a pulse at time T_0. This signal arrives at the receiver at time T_1, with amplitude V_{R1}. The receiver termination mismatch causes a signal reflection to travel back and arrive at the transmitter at time T_2. The transmitter termination mismatch then causes another reflection to travel back to the receiver, resulting in an
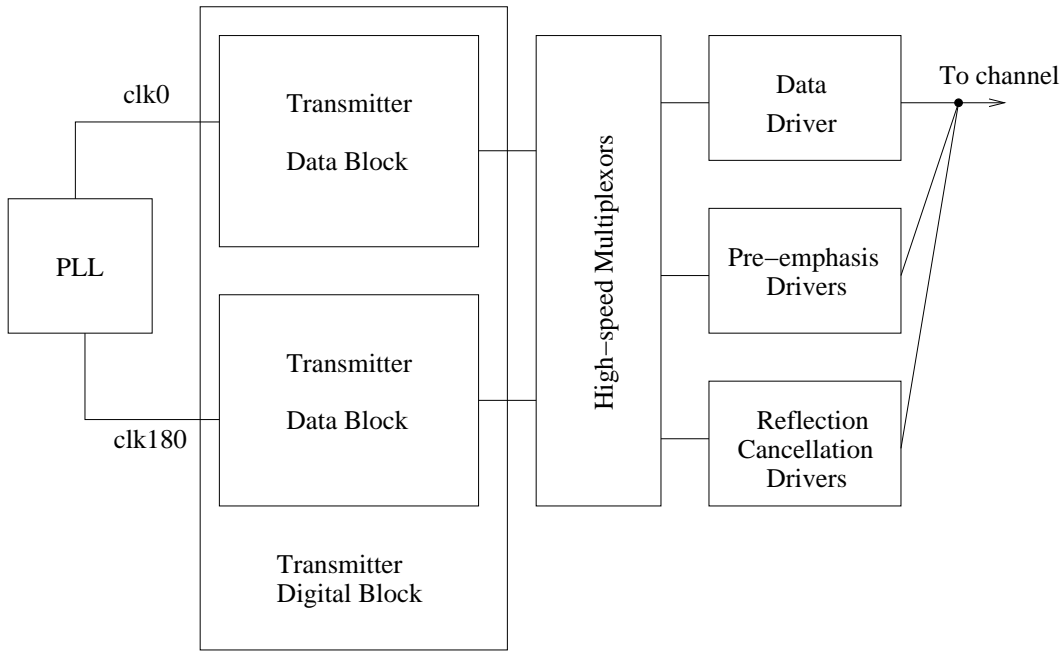
Figure 3.1: System overview.

undesired signal at the receiver at time T_3. The signal at time T_3 with an amplitude of V_{R3} is the interference that causes errors in signal detection.
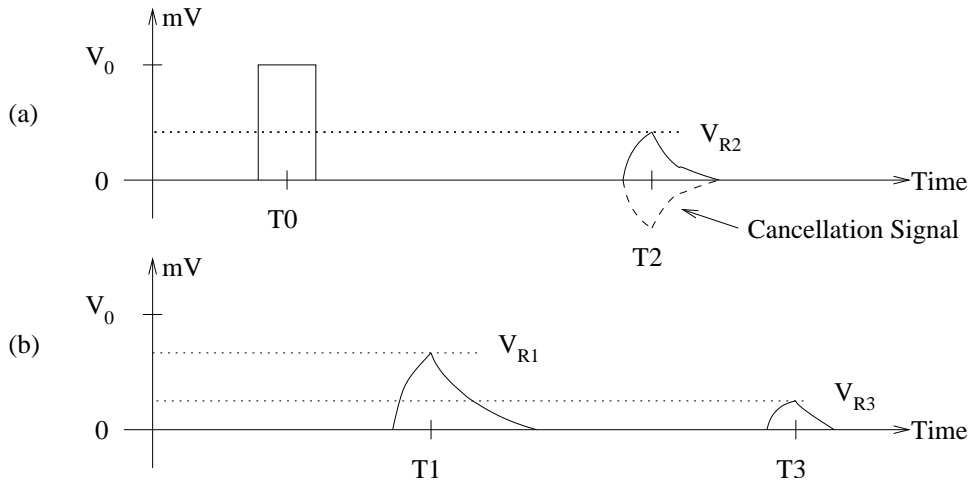
Figure 3.2: Approach to reflection cancellation. (a) Transmitter output. (b) Receiver input.

To remove the interfering signal, the reflection cancellation drivers sends out a negative

pulse at time T_2, as shown by the dashed line in Figure 3.2. The reflection canceling pulse, with an amplitude equal to the reflected portion of the signal traveling back to the receiver, cancels the reflection at the receiver. The reflection cancellation technique is able to cancel the reflections that are within the unit interval, regardless if they are coming from a resistive, a capacitive, or an inductive source.

The time resolution for the reflection cancellation is 1UI. This arrangement results in ease of implementation since the system clock can be used to create the 1UI delayed data. To design the reflection cancellation with a higher time resolution, a phase interpolation scheme is needed to shift the cancellation signals within unit intervals. Due to the time resolution limitation, any reflections that occur between unit intervals are only partially cancelled. However, this does not disrupt the reflection cancellation since reflections in the interval boundaries do not affect the vertical eye opening the most. The reflections in the middle of the unit intervals, which affect the vertical eye opening, are cancelled with the reflection-cancellation signals. Although this does not lead to perfect cancellation, it results in significant improvement of the eye opening as we will see later in Section 4.2.1.

3.2 Top Level Description

The top level block diagram of the transmitter is shown in Figure 3.3. The diagram includes all the major blocks inside the transmitter as well as their interconnections. There are three major blocks: the transmitter digital block, the transmitter front-end, and the PLL block. The transmitter digital block generates the data signals and passes them to the transmitter front-end for transmission. The data rate of the transmitter is $6Gbps$. The transmitter has a 3-tap pre-emphasis driver, which is adequate for a $1m$ PCB channel as shown in Section 2.5. For reflection cancellation, it has an 8-tap reflection canceller. This is an over-design as it was previous shown that only six taps are needed in typical backplane systems. However, eight taps do provide more flexibilities in dealing with complicated reflections. The PLL block provides the $3GHz$ clock signals for the transmitter digital block. These major blocks are discussed in detail later in this chapter.

All the data signals are differential. Throughout the thesis, the true and complement of a differential signal are named as *signal* and *signalx*. Also, *clk*0 and *clk*180 represent

the clock outputs of the PLL, while *clk* and *clkx* represent the clock signals within the transmitter digital block and the transmitter front-end. The clock signals *clk* and *clkx* are the buffered version of *clk*0 and *clk*180 respectively.
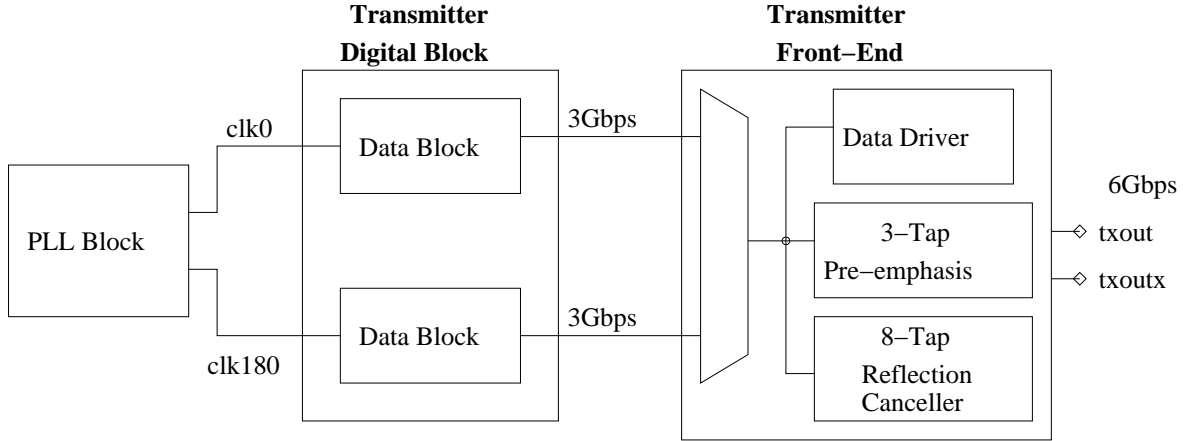
Figure 3.3: Top level block diagram.

3.3 Transmitter Digital Block

The transmitter digital block generates and processes the data for the transmitter front-end. Processing includes delaying, retiming, and inverting the data as required by the drivers in the transmitter front-end. The details of the transmitter digital block are shown in Figure 3.4. The digital block, consists of two data blocks, each operating on a different clock phase and providing one stream of half-rate data. The signals in the transmitter data block are differential, although they are shown as single-ended for simplicity throughout this chapter. In the transmitter data block, the data generator outputs data from either a $2^{31} - 1$ pseudo random bit sequence (PRBS) or a 128-bit user-defined sequence. The data generator output feeds into two paths, the main data path and the reflection data path. The data that goes through the main data path is not delayed, while the data in the reflection data path is delayed by 0 to 63 clock cycles (0 to 126 UIs) to match the timing of the reflections in the channel. This delay is enough to match the timing of the reflections in a 1*m* PCB channel with 6Gbps data rate.

There are two streams of data coming out from the dummy delay block *txdat*[1 : 0]. These streams are offset by one clock cycle. There are also four streams of data coming

Transmitter Digital Block
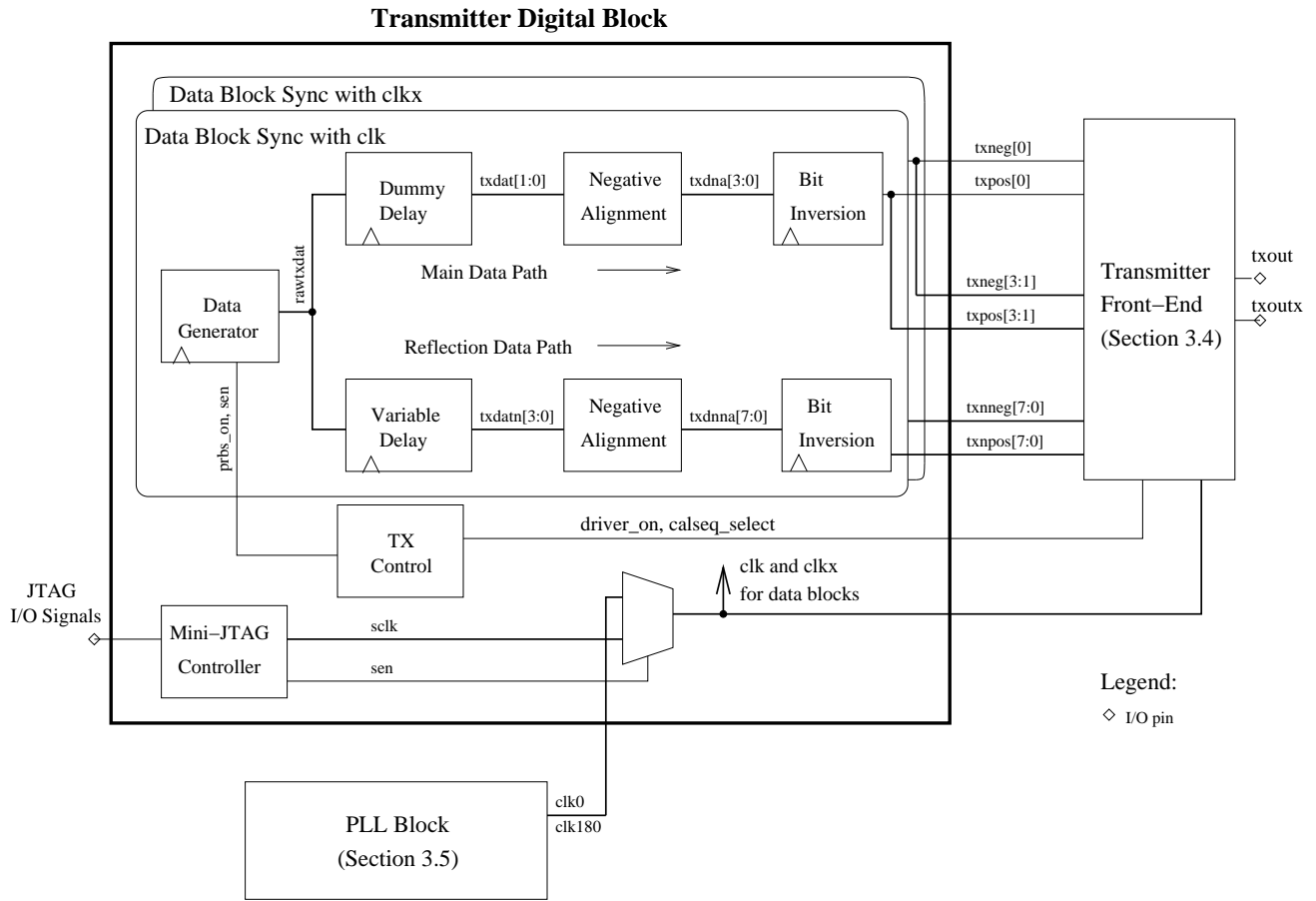
Figure 3.4: The transmitter digital block.

out of the variable delay block $txdatn[3:0]$, each with an additional clock cycle offset. These offset data streams are retimed in the negative alignment blocks with the opposite clock phase to produce 1/2 clock cycle (1UI) delayed data; data that is aligned with the positive clock edge is retimed to the following negative clock edge. At the output of the negative alignment block, two streams of output data, the original data stream and the retimed data stream, are produced for one stream of input. In Figure 3.4, two streams of data $txdat[1:0]$ becomes four output streams $txdna[3:0]$. These 1UI offset data streams then go through the bit inversion block. They are inverted, if needed, to allow the pre-emphasis drivers and the reflection-cancellation drivers in the transmitter front-end to produce negative cancellation signals. A total of twelve data streams, four from the main data path $txpos[3:0]$ and eight from the reflection data path $txnpos[7:0]$,

are ready for the transmitter front-end. The four data streams from the main data path go to the data driver, the 1st, 2nd and 3rd pre-emphasis drivers, while the eight data streams from the reflection data path go to the eight reflection-cancellation drivers.

A control block and a mini-Joint Test Action Group (JTAG) controller are also included in the transmitter digital block. The scan-clock *sclk* coming out of the mini-JTAG scan-chain control block is sent to all the blocks that are in the scan-chain, which will be discussed later in the chapter. The flip-flops of the data generator and those blocks with the up-arrow sign use the system clock, *clk* and *clkx*. The system clock is multiplexed between the scan-clock and the PLL clock, and one of them is selected depending on the operation mode. The operation modes of the transmitter are covered in Chapter 4. The sub-blocks of the transmitter digital block are discussed next.

3.3.1 Data Generator

The data generator, as shown in Figure 3.5, is made up of 128 cascaded flip-flops that are connected in a ring architecture. The implementation of the flip-flops is discussed later in Section 3.6.1. The 3-to-1 multiplexor, with a pair of control inputs, *prbs_on* and *sen*, selects one of the three functions of the data generator:

1. A section of the scan-chain in the transmitter

2. $2^{31} - 1$ Pseudo Random Bit Sequence (PRBS) generator

3. 128-bit circular shift register

Table 3.1 lists the data generator inputs and their corresponding functions. When input *sen* is high, the data generator goes into scan-in mode and hence *prbs_on* is ignored. This generator architecture requires the least number of flip-flops to implement all three functions since the PRBS generator shares the flip-flops with the 128-bit circular shift register. The scan-chain within the data generator starts at the multiplexor *sin* and ends at the 32nd flip-flop *sout*. The operation of the scan-chain is described later in Section 3.3.7.

In the PRBS mode, the last thirty-one flip-flops are used to generate a $2^{31} - 1$ PRBS with the initial seed pre-loaded during the scan-in process. Inputs to the XOR gate are tapped from bit 0 and bit 3. Only two bits are chosen as the inputs to the XOR gate because they are the minimum required to ensure that a maximum length sequence is
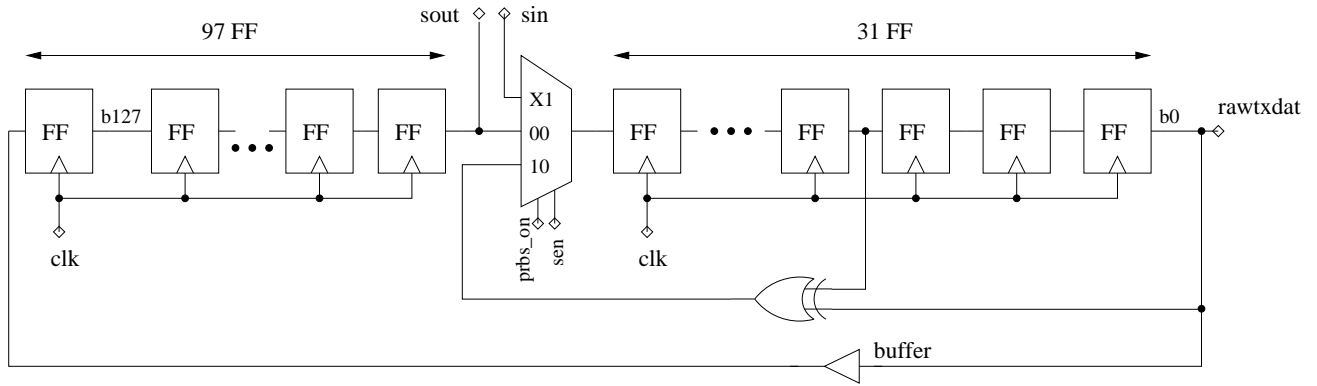
Figure 3.5: The transmitter data generator.

Table 3.1: Data generator functions.

prbs_on	*sen*	Functions
0	0	128-bit circular shift register
X	1	Scan-in mode
1	0	$2^{31} - 1$ PRBS

produced. As a result, the generator polynomial implemented is $X^{32} + X^3 + 1 = 0$. Part of the resulting bit stream is shown in Table 3.2.

Table 3.2: PRBS sequence example.

State (b_{30} to b_1)	Output *rawtxdat*
00000000000000000000000001000	1
10000000000000000000000000100	0
11000000000000000000000000010	0
01100000000000000000000000001	0
00110000000000000000000000000	1

The 128-bit circular shift register is used for the transmission of the custom input sequence and the calibration sequence. During this mode, the pre-loaded data is sent out repeatedly. A long metal wire is required to connect the bit 0 flip-flop and the bit 127 flip-flop; thus, the last flip-flop has to drive the wiring capacitance of the long metal wire as well as the input capacitance of the next stage. The buffer inserted in the feedback

path reduces the wiring capacitance that the last flip-flop has to drive. The outputs of the data generator are fed to the main data path and the reflection data path.

3.3.2 Variable Delay Block

The variable delay block is used to generate the delayed version of the transmitted data for the reflection-cancellation drivers. It has a 6-bit input from the scan-chain and can delay the data by 0 to 63 clock cycles. Two possible implementations of the variable delay block with only 2-to-1 multiplexors and flip-flops are shown in Figure 3.6. The implementation in Figure 3.6(a) gives a constant delay path between the input and the output, regardless of the delay selection. The delay path for this implementation is always one multiplexor. However, the data input loading of this implementation can be large since the input signal routes to all the multiplexors and one flip-flop.

We have chosen the implementation in Figure 3.6(b). This particular implementation has the least amount of data input loading, that is one multiplexor and one flip-flop. This increases the maximum operating speed of the data path since little buffering is required for the data.

The disadvantage of this implementation is that the data goes through six multiplexors in one clock cycle when zero delay is selected. Since the clock period is only $333ps$, it is impossible to meet the timing requirement with this implementation. To relax the timing requirement, the data path is divided into three pipeline stages by the use of two multiplexor flip-flops, labelled as "MUX Flip-flop" in Figure 3.6(b). The "MUX flip-flop" is equipvalent to a 2-to-1 multiplexor cascaded by a flip-flop. The implementation of the "MUX flip-flop" is described later in Section 3.6.2.

The transmitter has eight reflection-cancellation drivers, which require eight streams of data with 1UI spacing in the reflection data path. The four flip-flops at the output of the variable delay block provide four data streams with one clock cycle spacing, and the four data streams are further divided into the eight data streams with 1UI spacing in the next stage. The output waveforms of the variable delay block are shown in Figure 3.7.
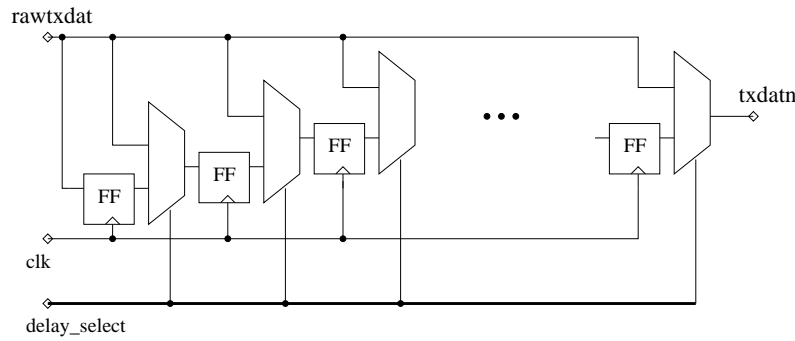
(a)
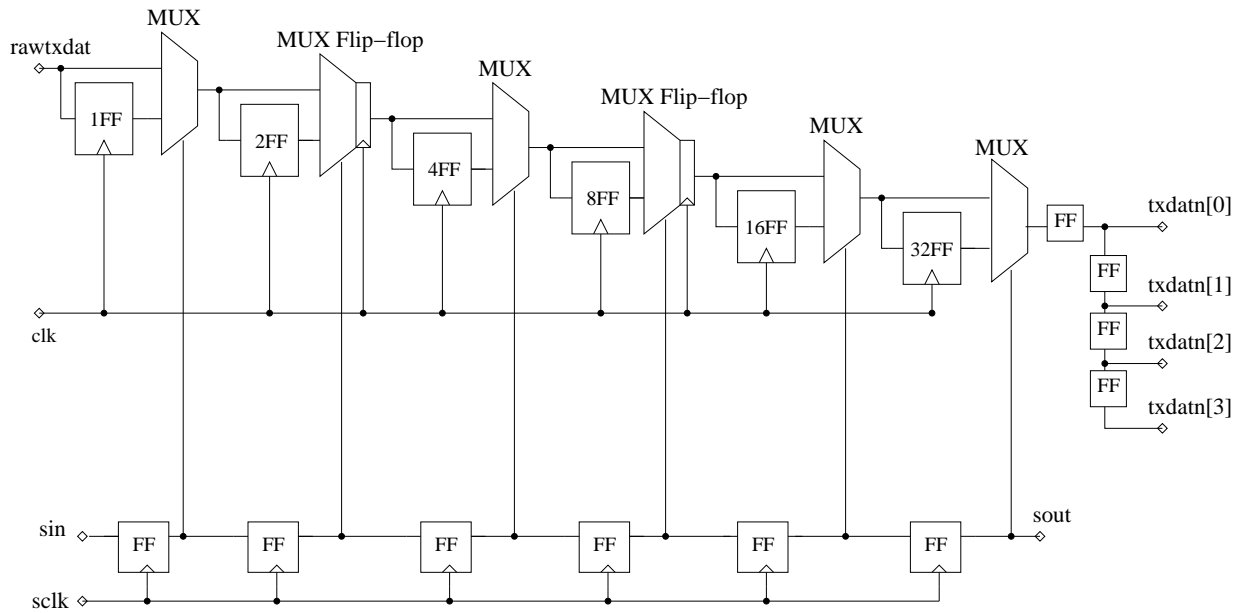
(b)

Figure 3.6: Variable delay block implemented with only 2-to-1 multiplexors and flip-flops. (a) Implementation with constant delay but large input loading. (b) Implementation with long zero-delay path but small input loading.

3.3.3 Dummy Delay Block

Since two multiplexor flip-flops are used in the variable delay block, two flip-flops are inserted in the dummy delay block to align the main data path to the innate pipeline delay of the variable delay block. The dummy delay block is shown in Figure 3.8.
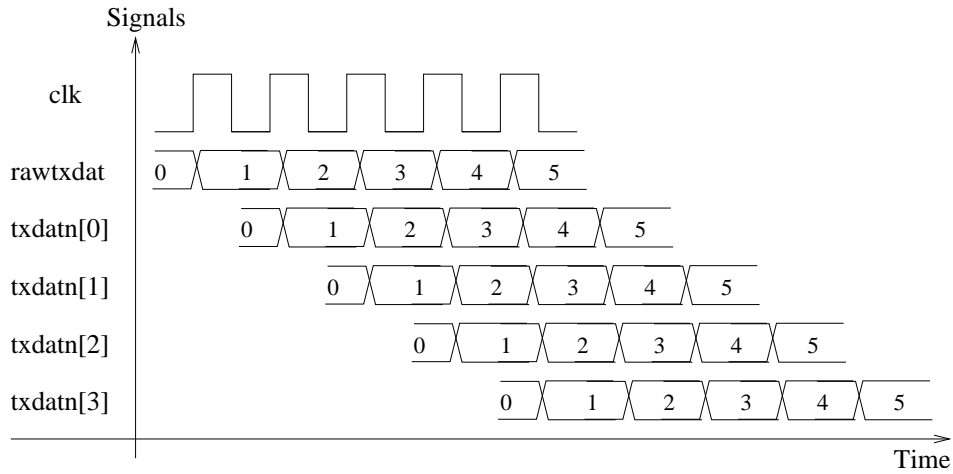
Figure 3.7: The timing diagram of the signals in the variable delay block.
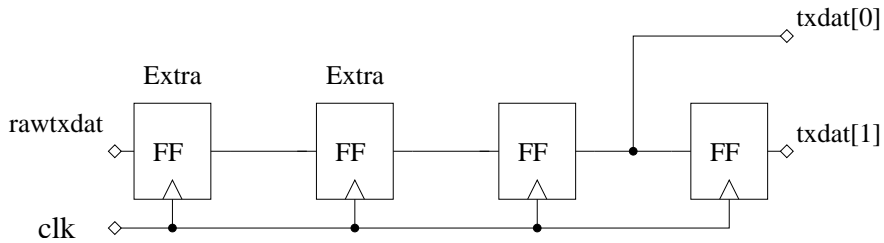
Figure 3.8: The dummy delay block.

The main data path provides the data for the data driver and the three pre-emphasis drivers. The data from $txdat[0]$ is later split into 0UI and 1UI delayed data for the data driver and the 1st pre-emphasis driver. The data from $txdat[1]$ is delayed by one clock cycle from $txdat[0]$ and will be split into 2UI and 3UI delayed data for the 2nd and the 3rd pre-emphasis drivers.

3.3.4 Negative Alignment Block

The purpose of the negative alignment block is to realign the input data stream with the opposite clock phase to create a 1UI delayed version of the input data. The block diagram for the negative alignment block is shown in Figure 3.9.

To create a 1UI delayed version of the incoming data stream, the output of the first flip-flop is fed into the second negative edge triggered flip-flop. The output $dout0p5$ is
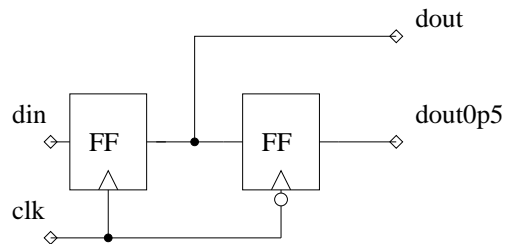
Figure 3.9: The negative alignment block.

retimed to the negative edge of the clock, which is 1UI delayed from the output *dout.*
The timing diagram of the operation is shown in Figure 3.10.
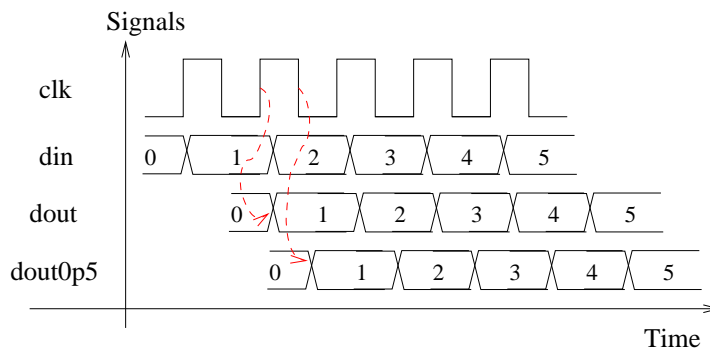
Figure 3.10: The negative alignment block timing diagram.

3.3.5 Bit Inversion Block

The bit inversion block inverts the data stream so that the pre-emphasis drivers and
reflection-cancellation drivers can create negative cancellation signals. The schematic of
the bit inversion block is illustrated in Figure 3.11.

The circuit is a 2-to-1 multiplexor. The implementation of the multiplexor is described
later in Section 3.6.3. The bit inversion block selects either *txdat* or its inverted value
from the incoming data stream, with the select input of the multiplexor coming from
the scan-chain. The differential implementation of the bit inversion block eliminates the
inverter by flipping the differential wires.
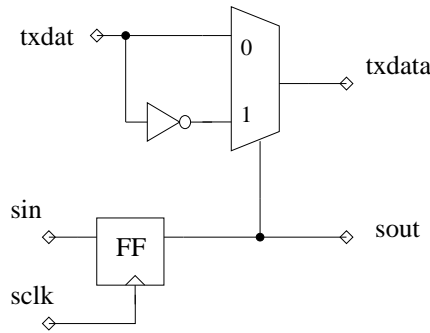
Figure 3.11: The bit inversion block.

3.3.6 The Scan Mechanism and the Mini-JTAG Controller

The transmitter has a large number of parameters controlling the operation of the ISI and reflection cancellation processes. It would be ideal to provide I/O pins for all the parameters such that they are controlled easily, however, such a setup would not be feasible given the limited number of I/O pins on the chip. Thus, a scan-chain is designed to scan the parameters into the transmitter serially. An overview of the scan mechanism in the transmitter is shown in Figure 3.12. The mechanism consists of a mini-JTAG controller, a scan-clock enable logic, and a scan-chain. The mini-JTAG controller enables the scan-clock with signal *sen*. Two blocks are shown with scan input, one has 3 parameter bits and the other has 2 parameter bits. The scan-data enters the scan-chain from *tdi* with each scan-clock cycle until the whole scan-chain is filled. The output of the flip-flops hold the scan-data, which are the paramters needed for the circuit blocks. This scan mechanism is made compliant to the JTAG standard for the ease of testing. JTAG is an Institute of Electrical and Electronics Engineers (IEEE) standard for boundary testing of ICs that allows using the least number of I/O pins to test the functions of the chip [IEE93]. There are four input pins and one output pin in the JTAG standard as listed in Table 3.3.

The mini-JTAG controller is an Finite State Machine (FSM) that is compatible with standard JTAG testers. However, the mini-JTAG controller implements only the JTAG functions required in the transmitter, such as shifting in and out of data. The controller FSM as shown in Figure 3.13 has seven states, which are the minimum required to be compatible with JTAG testers. The FSM moves from state to state depending on input *tms*, which is a bit stream that is aligned with JTAG clock *tck*. The FSM states and
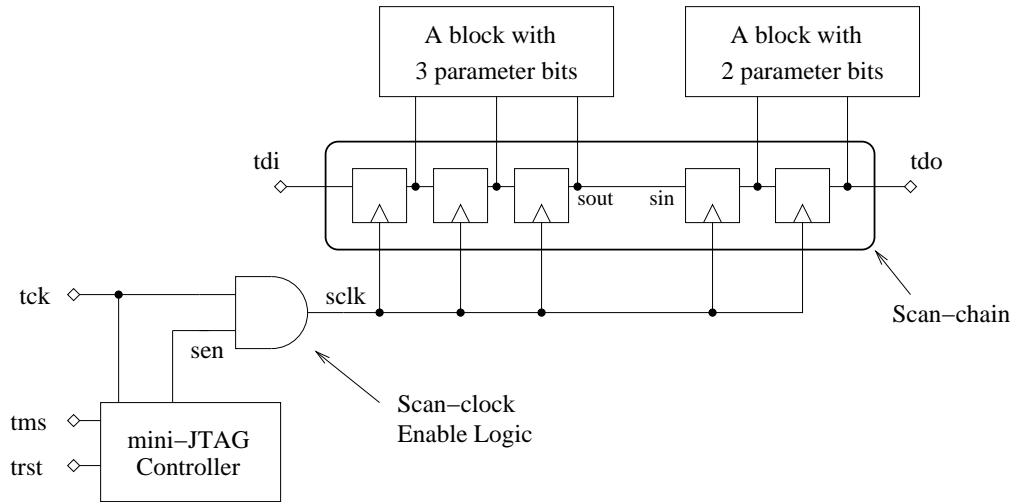
Figure 3.12: Overview of the scan mechanism in the transmitter.

Table 3.3: JTAG pin list.

Pin Name	Direction	Functions
tdi	Input	Scan-data input
tck	Input	JTAG clock
tms	Input	Test mode select
trst	Input	JTAG reset (optional)
tdo	Output	Scan-data output

their functions are listed in Table 3.4. State ShDR enables the data scan-in by setting *sen* to high, while the other states disable the scan-in process by setting *sen* to low. The scan-clock *sclk* is a gated version of the JTAG clock *tck*; the gating is provided by an AND-gate with *sen* being the enable signal. The signal *trst* is the signal to reset the mini-JTAG controller back to the TLR state. The actual scan-chain is a chain of flip-flops with a single input *tdi* and a single output *tdo*. In the transmitter, the input and output of scan-chain sections within circuit blocks are named as *sin* and *sout* respectively.
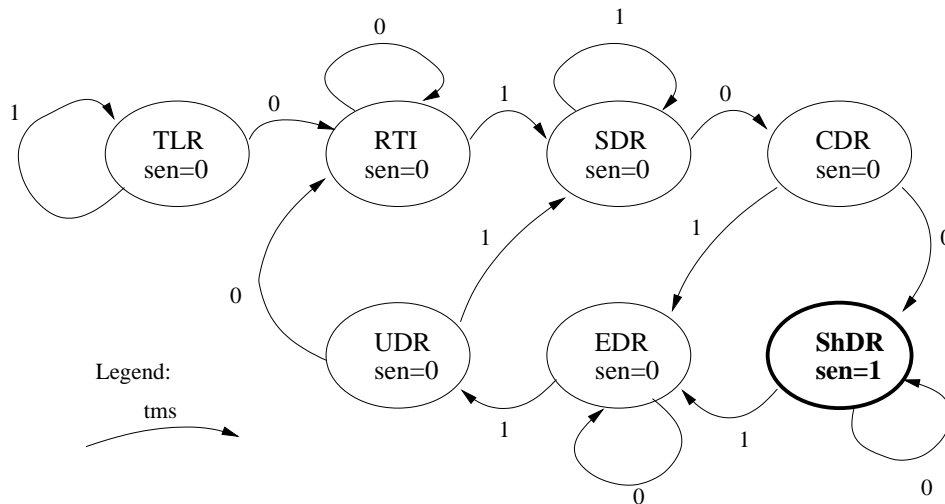
Figure 3.13: The mini-JTAG controller FSM.

Table 3.4: FSM states representation and output.

	State			Output	
State Name	q_2	q_1	q_0	sen	Function
TLR	0	0	0	0	Reset state machine
RTI	0	0	1	0	Idle state
SDR	0	1	0	0	Do nothing
CDR	0	1	1	0	Do nothing
ShDR	1	0	0	1	Shift data in and out of the chip
EDR	1	0	1	0	Do nothing
UDR	1	1	0	0	Do nothing
Not Used	1	1	1	0	

3.3.7 Scan-Chain

The scan-chain in the transmitter is shown in Figure 3.14. It goes through the major blocks in the transmitter and sets the parameters for the blocks. The first section of the scan-chain is in the data block synchronized with clk. The first part of the scan-chain is the 128 flip-flops in the data generator. These flip-flops are shared between the data path and the scan-chain since their initial states are set by the scan-in process. The next part of the scan-chain is inside the variable delay block and it sets the 6-bit delay control

bit (MSB to LSB). The next section of the scan-chain sets the 8-bit and 4-bit invert control signals for the reflection data path and the main data path. The scan-chain then repeats itself for the data block that is synchronized with *clkx*. Next, the scan-chain sets the 6-bit tap strength control (MSB to LSB) for the pre-emphasis drivers and the reflection-cancellation drivers, starting with the 1st pre-emphasis driver and ending with the 8th reflection-cancellation driver. The last two bits of the scan-chain are inside the transmitter control block to set the transmitter operation mode as described in Section 3.3.8. Table 3.5 shows the bits assignment of the scan-chain in detail.
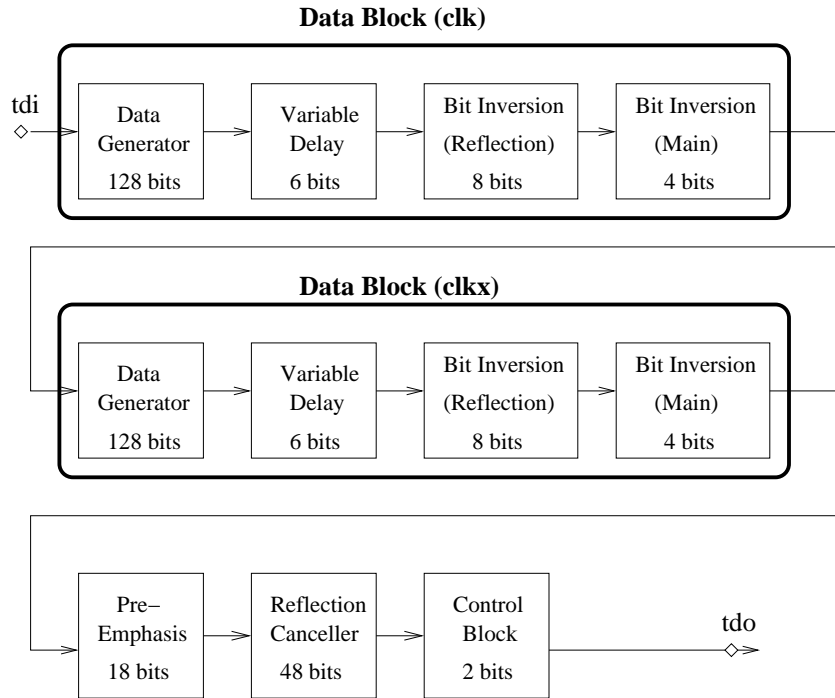
Figure 3.14: The transmitter scan-chain.

3.3.8 Transmitter Control Block

The transmitter control block contains the control logic for the transmitter. It controls the data driver, the data generator, and the calibration sequence enable pin in the high-speed data multiplexors. The block diagram of the control block is shown in Figure 3.15.

The last two bits of the scan-chain are located in the transmitter control block, *prbs*

Table 3.5: Detailed scan-chain bit representation.

Bits	Function Block	Description
359:232	Data Generator	128-bit data generator
231:226	Variable Delay	6-bit delay chain
225:218	Bit Inversion	8-bit invert signal (reflection data path)
217:214	Bit Inversion	4-bit invert signal (main data path)
213:86	Data Generator	128-bit data generator
85:80	Variable Delay	6-bit delay chain
79:72	Bit Inversion	8-bit invert signal (reflection data path)
71:68	Bit Inversion	4-bit invert signal (main data path)
67:50	3-tap Pre-emphasis	3 6-bit pre-emphasis tap control
49:2	8-tap Reflection Canceller	8 6-bit reflection tap control
1:0	TX Control Block	*prbs* and *calibration* bits
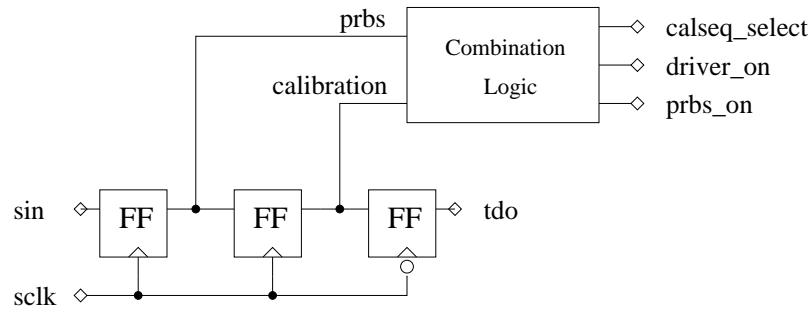
Figure 3.15: The transmitter control block.

and *calibration*, and they are the only inputs to the combinational logic. Table 3.6 shows the truth table of the inputs and their corresponding outputs and functions. The output *prbs_on* is the PRBS select signal for the data generator, *driver_on* is the enable signal for the transmitter drivers, and *calseq_select* is the calibration sequence enable signal in the high-speed data multiplexors.

3.3.9 Transmitter Digital Block Layout

A testchip of the transmitter is implemented in Fujitsu's $0.11\mu m$ CMOS process. The layout of the transmitter digital block in the transmitter testchip is shown in Figure 3.16. The size of the layout is $550\mu m \times 300\mu m$. The digital block synchronized by *clkx*

Table 3.6: Transmitter control logic truth table.

Inputs			Outputs		
prbs	*calibration*	Operation Mode	*prbs_on*	*driver_on*	*calseq_select*
0	0	Custom Input	0	1	0
0	1	Calibration	0	1	1
1	0	PRBS	1	1	0
1	1	Driver Off	0	0	0

is at the top while the one synchronized by *clk* is placed at the bottom. The clock buffer is placed in the middle of the chip. The negative alignment blocks and the bit inversion blocks are placed after the delay blocks, and the data multiplexors, discussed in later in Section 3.4.1, are placed in the right. In addition, the transmitter control logic is placed at the bottom. The layout is optimized such that minimum length of wiring is needed to connect the digital block to the transmitter front-end.
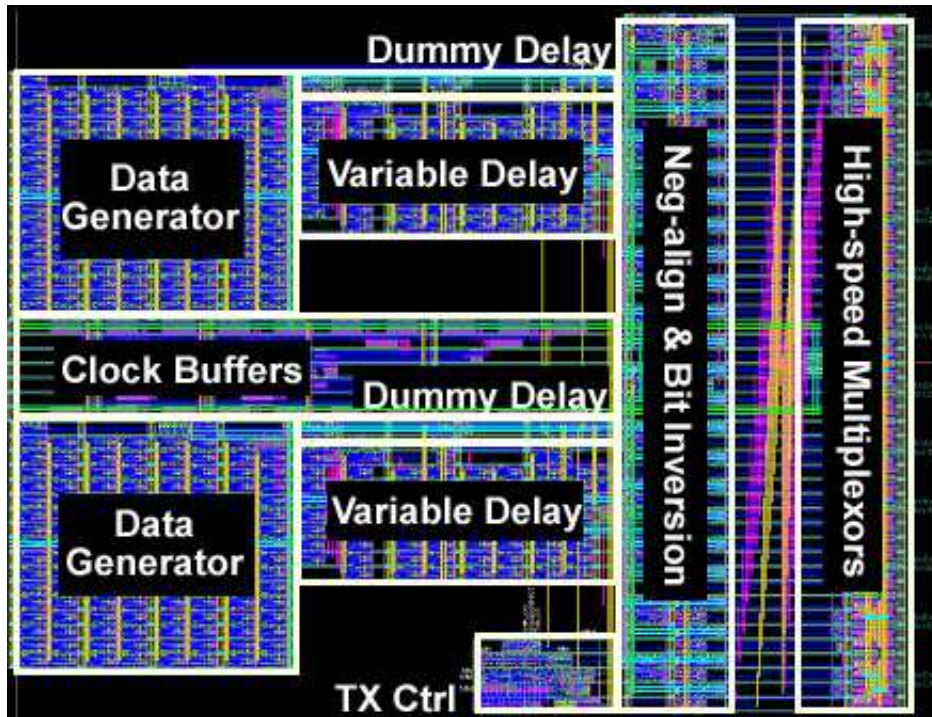
Figure 3.16: Transmitter digital block layout.

3.4 The Transmitter Front-End Block

The transmitter front-end, as shown in Figure 3.17, combines and transmits the data from the digital block. Besides the normal data transmission, the transmitter front-end provides ISI and reflection cancellation. In the transmitter front-end, there are six blocks: the high-speed data multiplexors, the driver bias circuit, the data driver, the 3-tap pre-emphasis driver, the 8-tap reflection canceller, and the 4-bit digitally controlled variable termination resistors. The high-speed data multiplexors merge the data from the transmitter digital block into a 6Gbps data stream. The data driver then transmits the data stream onto the channel. The channel output is a current sum of the signals from the data driver, the 3-tap pre-emphasis driver, and the 8-tap reflection canceller. The 8 continuous taps of the reflection canceller can be delayed from 0 to 126 UIs to match the timing of the reflections. The delay is provided by the variable delay block, which was described in Section 3.3.2. The bias voltages of the current sources for all the drivers are provided from a common bias circuit. To properly terminate the channel at the transmitter end, a pair of 4-bit externally controlled PMOS resistors are implemented. The following sections discuss the sub-blocks of the transmitter front-end in detail.

3.4.1 High-Speed Data Multiplexor

High-speed multiplexors merge the data generated by the two transmitter data blocks into a 6Gbps data stream for transmission. The data inputs to the data multiplexor, *txpos* and *txneg*, in Figure 3.18 come from the output of the transmitter digital block. The same data multiplexor is used for the complement of the differential data. Inputs *txpos* and *txneg* are the 3Gbps data streams synchronized with the *clk* and *clkx* respectively. Signals *invpos* and *invneg* in Figure 3.18 are enable signals for the calibration mode. The calibration mode requires a zero symbol to obtain the channel characteristics. The zero symbol has a voltage level midway between a '1' symbol and a '-1' symbol. The calibration mode is discussed later in Chapter 4. Table 3.7 shows the truth table for the *invpos* and *invneg* signals. Input signal *invert* comes from the bit inversion block in the transmitter digital block and input *calseq_select* comes from the transmitter control block. If either the *invpos* or the *invneg* signal is pulled low, the transmitter goes into the calibration mode. All the '-1' symbols are converted into zero symbols by disabling
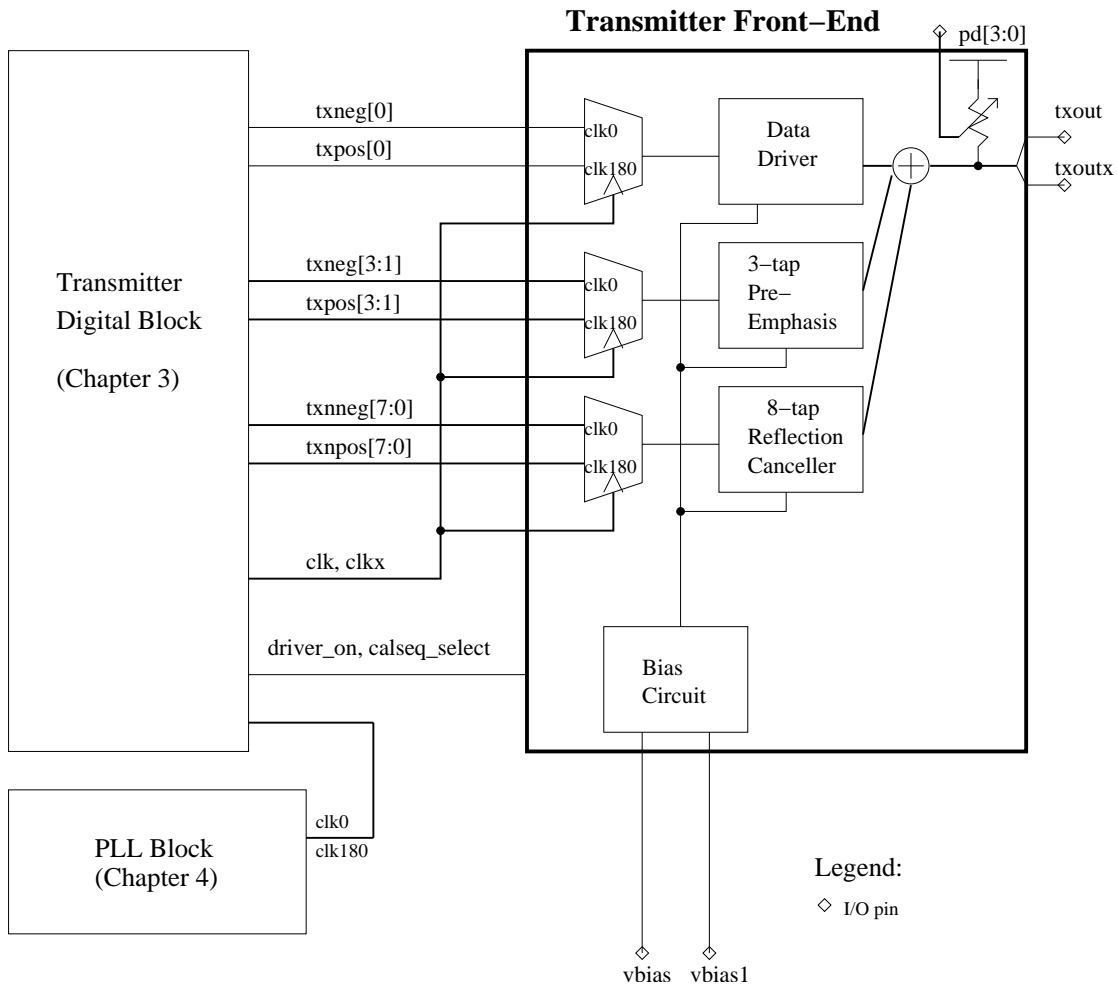
Figure 3.17: The transmitter front-end block.

both the true and complement data in the data multiplexors. Thus, the data inputs to the differential pair drivers will have the same voltage and produce the zero symbol.

There are two parallel branches in the data multiplexor, one selected by *clk* and the other one selected by *clkx*. The ideal time for the multiplexor to sample the 3Gbps data is in the middle of the data period. Thus, the positive edge of *clkx* is used to select the data that is aligned to *clk*. The timing diagram can be seen in Figure 3.19. When *clk* is high, the net *muxout* is pulled low if signal *txneg* is high. Thus, this is an inverting multiplexor. The signal at *muxout* goes through a pre-driver before reaching the drivers. The purpose of the pre-driver is to level shift the signals so that they are suitable for the drivers. The signal swing at the output of the data multiplexor is V_{DD} to $800mV$.

Table 3.7: Truth table for data multiplexor *invpos* and *invneg* pins.

Input		Output		
invert	*calseq_select*	*invpos*	*invneg*	Functions
0	0	1	1	Normal transmission
0	1	1	0	Calibration mode
1	0	1	1	Inverted normal transmission
1	1	0	1	Invert calibration mode
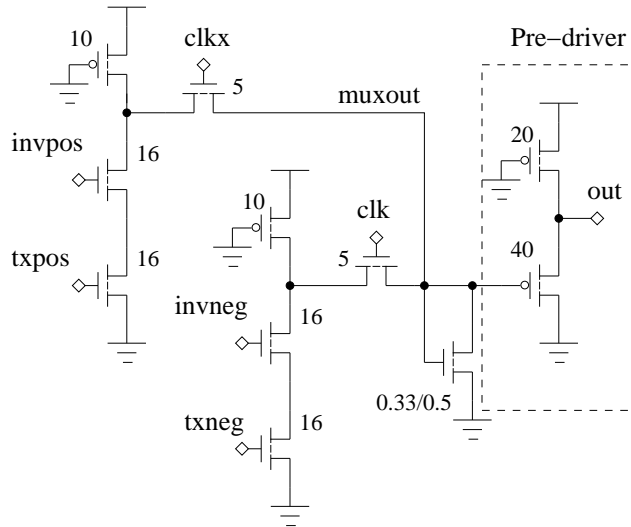
Note: All transistor lengths are 0.11um unless indicated otherwise

Figure 3.18: The 6Gbps high-speed data multiplexor.

Simulation results show that the multiplexor output signal swing can fully switch the current in the drivers.

3.4.2 Bias Circuit

A wide-swing cascode bias circuit [JM97] is used to provide the bias voltage for the current sources of the data driver, the pre-emphasis drivers and the reflection-cancellation drivers. This bias circuit has a simple implementation yet it provides a high output impedance. The circuit is shown in Figure 3.20.

There are two inputs to this circuit, *vbias* and *vbias1*, and they both require an

Signals

clk

clkx

txpos | 0 | 2 | 4 | 6 | 8 | 10

txneg | 1 | 3 | 5 | 7 | 9 | 11

txout | 1 | 2 | 3 | 4 | 5 | 6 | 7 | 8 | 9

Time
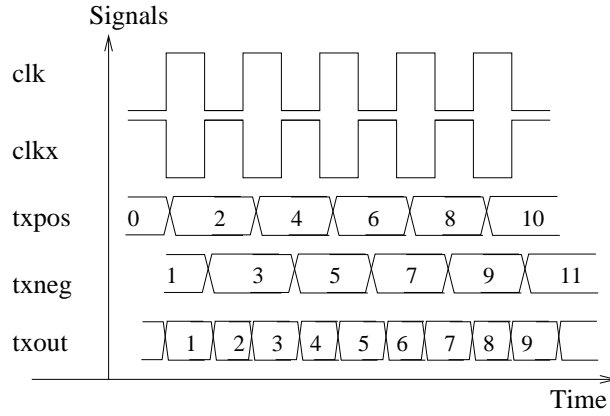
Figure 3.19: Timing diagram of the high-speed data multiplexor.

vbias   vbias1

n_bias   n_upper

1.25   5

n_lower

5
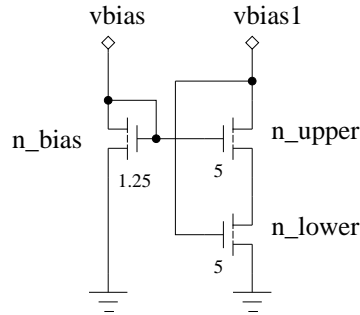
Note: All transistor lengths are 0.11um.

Figure 3.20: The wide-swing cascode bias circuit for data driver.

external current input of $250uA$. The voltage output at *vbias* is $750mV$ and at *vbias1* is $478mV$. The bias voltages are designed such that the transistor *n_lower* is at the edge of saturation, which results in the maximum voltage swing at the driver output.

3.4.3 Driver Circuits

The 6Gbps data driver is illustrated in Figure 3.21. The data driver is a differential amplifier with variable resistors as the output loads. The width of the differential NMOS pair is $100\mu m$. Since there are twelve differential pairs (one data driver, three pre-emphasis drivers, and eight reflection-cancellation drivers) connected together, the design is try to balance between the resulting output capacitance and the bandwidth of

the driver. Simulation result shows that the $100\mu m$ differential pair is able to produce output signal at 6Gbps while minimizing the output capacitance. The variable resistors are implemented by fifteen PMOS fingers with a 4-bit off-chip digital control as shown in Figure 3.22. The four bits are binary weighted among the fifteen PMOS fingers. For instance, code 0000 turns on all fifteen fingers, while code 1100 turns on three fingers. The obtainable resistance range is between 25Ω to 700Ω. To obtain 50Ω in the typical process, code 0100 is required externally.
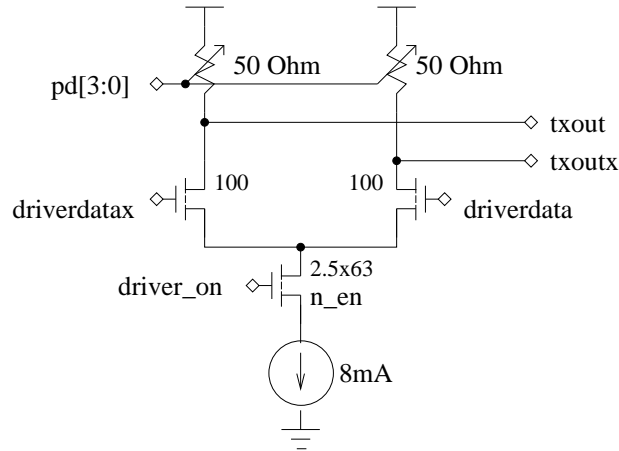
Note: All transistor lengths are 0.11um

Figure 3.21: The data driver.
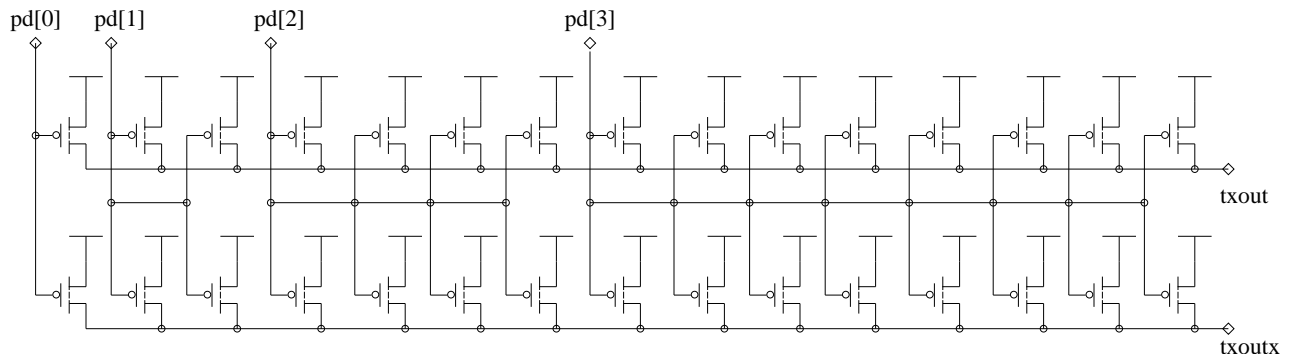
Figure 3.22: The 4-bit controlled variable termination resistor.

The current source for the data driver as shown in Figure 3.23 sinks $8mA$ of current. The size of the NMOS is thirty-two times the size of the NMOS in the bias circuit.

The $8mA$ current produces an output swing of $200mV$ in a 50Ω channel. The $200mV$ transmitted signal swing is the minimum required to produce a $100mV$ received signal at the end of a $10m$ PCB trace at a data rate of 6Gbps. Transistor n_en is the enable switch for the data driver. When the driver is on, transistor n_en is a small resistor and does not interfere with the driver's operation.
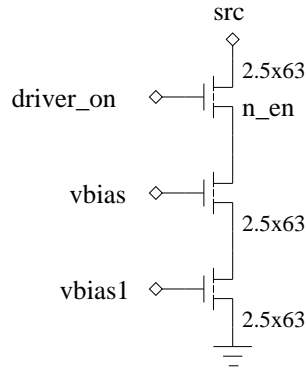
Note: All transistor lengths are 0.11um

Figure 3.23: The current source for the data driver.

The schematics for the 3-tap pre-emphasis driver and 8-tap reflection-cancellation driver are shown in Figure 3.24 and Figure 3.25 respectively. They are also implemented by differential amplifiers. The current sources for the pre-emphasis drivers and the reflection-cancellation drivers are different from the data driver as shown in Figure 3.26. The $8mA$ current is divided into six binary weighted branches, and each branch has a similar structure to the data driver current source. The $8mA$ current is an over-design for the pre-emphasis drivers and the reflection cancellation drivers because ISI and reflections cancellation signals normally have amplitude much less than the data signals. However, the use of the same current source as the data driver saves design time in the layout stage as it can be copied directly from the data driver current source. The enable transistors are controlled by the scan-chain outputs.
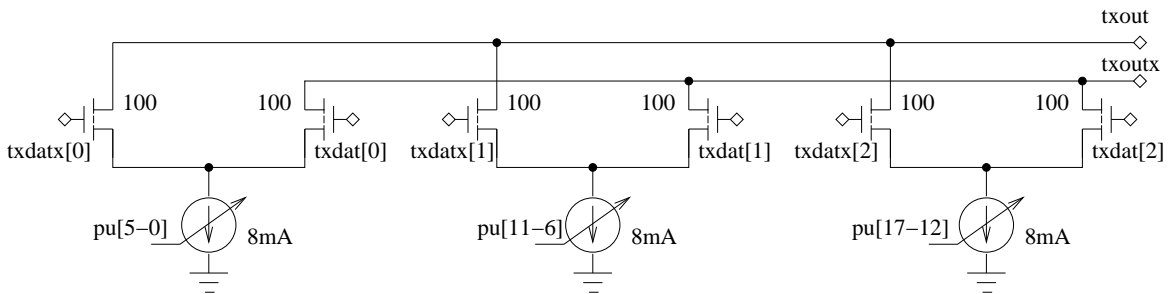
Figure 3.24: The 3-tap pre-emphasis driver.
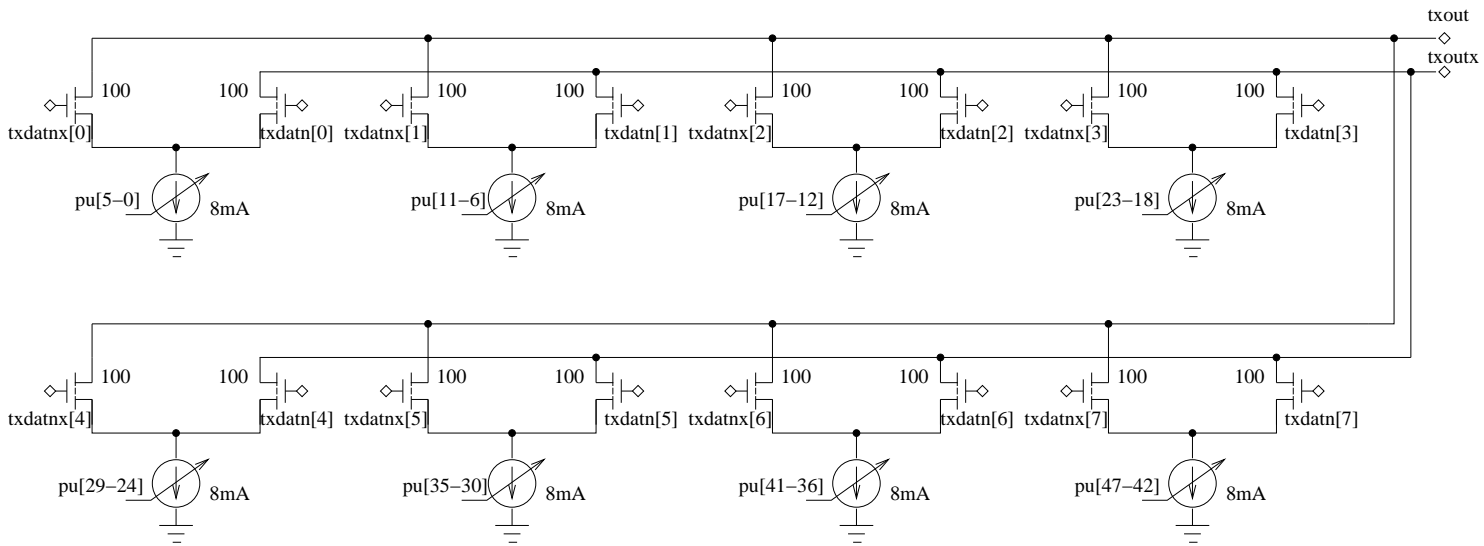
Figure 3.25: The 8-tap reflection-cancellation driver.
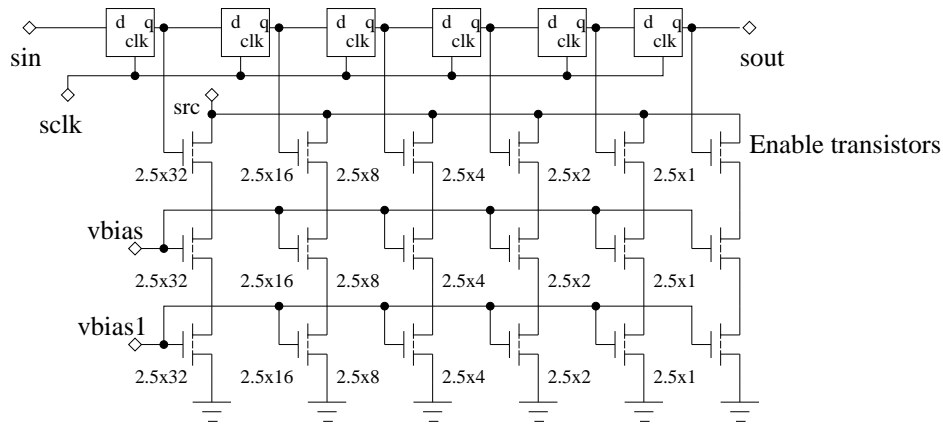
Note: All transistor lengths are 0.11um

Figure 3.26: The current source for the pre-emphasis drivers and reflection canceller.

3.4.4 Transmitter Front-End Layout

The layout of the transmitter drivers in the transmitter testchip is illustrated in Figure 3.27. The driver circuits have an area of $250\mu m \times 300\mu m$ and occupy five I/O pad sites. The high-speed differential output pins *txout* and *txoutx* are placed between power supply pins to provide signal return paths. The current sources and bias circuit are placed below the driver circuits.

3.5 Phase Locked Loop

A PLL is designed as a clock generator to synchronize the sequential circuits in the transmitter digital block and to drive the high-speed multiplexors in the transmitter front-end. The PLL block as shown in Figure 3.28 has seven major blocks: the phase-frequency detector (PFD), the charge pump, the loop filter, the voltage controlled oscillator (VCO), the clock divider, and the asynchronous enable block [Raz01] [JM97]. The control signal *pllen* selects between the VCO clock output and the bypass clock *bypclk*. The final outputs of the PLL are two $3GHz$ clock signals: *clk*0 and *clk*180.

The PFD and the charge pump are implemented as the charge pump phase comparator [JM97]. The PFD is a sequential phase detector based on NOR gates. The relationship between the average current generated by the charge pump and the phase difference of
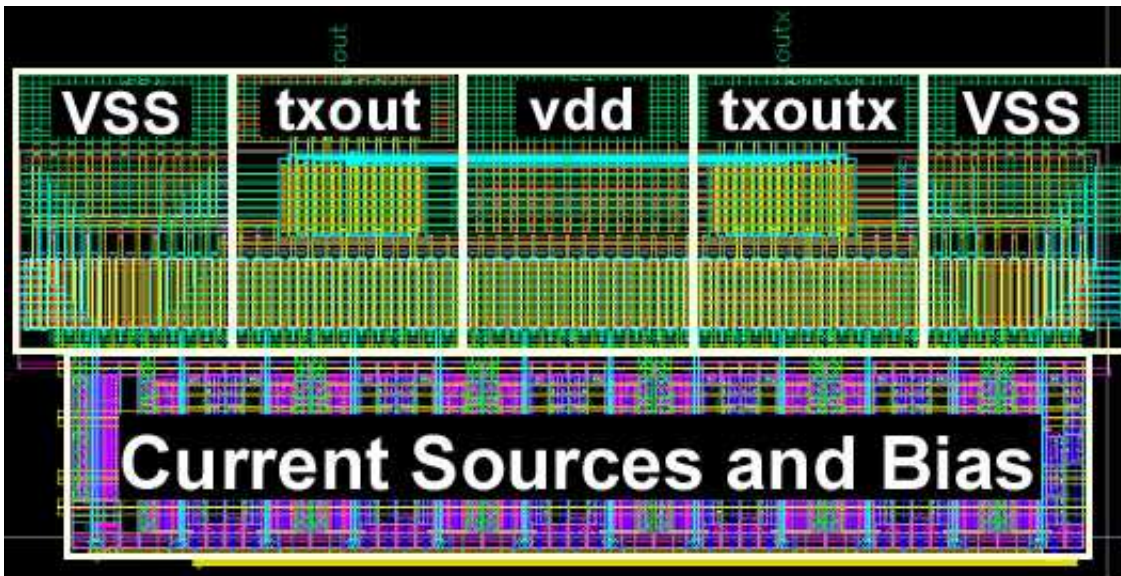
Figure 3.27: Transmitter front-end layout.
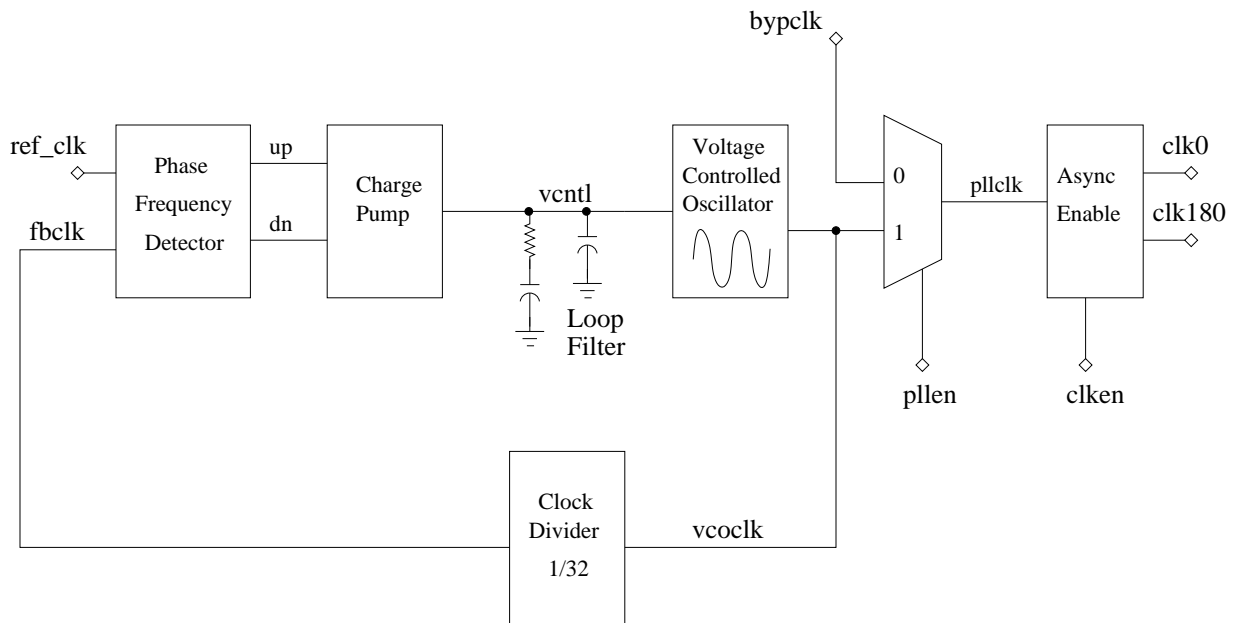
Figure 3.28: Top level PLL diagram.

the feedback and the reference clocks is simulated in Hspice. The plot is shown in Figure 3.29. The slope of the line represents the gain of the charge pump phase comparator,

which is equal to $9.86uA/rad$ in the typical process corner.
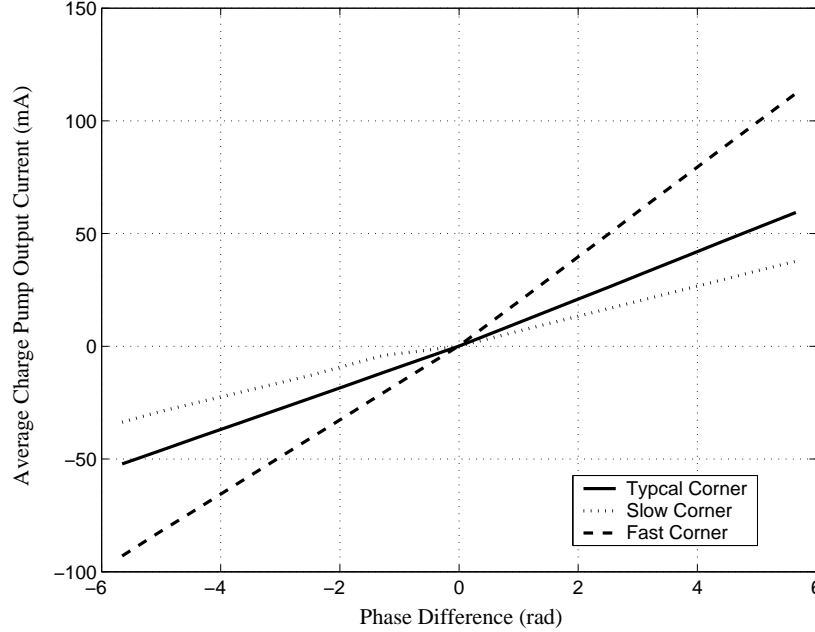
Figure 3.29: Relationship between charge pump current and phase difference between ref_clk and fb_clk.

The loop filter is a second order passive filter [Raz01]. A PLL needs to have damping factor $\zeta = 0.707$ to 1 for its transient response to be critically damped. For this loop filter, ζ is designed to be 0.8915. With this loop filter, the bandwidth of the PLL is $11.7MHz$.

The oscillator of the PLL is a tuned LC-VCO modified from [AM00] as shown in Figure 3.30. It is implemented with an inductor, a varactor, and a negative Gm stage. The inductor has an inductance of $1nH$. The varactor is implemented with NMOS transistors with their drain and source nodes shorted together. The VCO has a centre frequency of $3GHz$. The range of the control voltage goes from $0V$ to $1.2V$, with a linear tuning region between $0.3V$ to $0.9V$. As shown in Figure 3.31, the tuning range of the VCO is between $2.5GHz$ to $3.8GHz$. The gain of the VCO, K_{VCO}, is equal to the slope of the tangent line at $V_{cntl} = 0.6V$. In the typical process corner, the gain of the VCO is $1.66GHz/V$.

In this PLL, the VCO clock frequency is divided by thirty-two using five cascaded flip-flops. The clock divider schematic is shown in Figure 3.32. The challenge in this
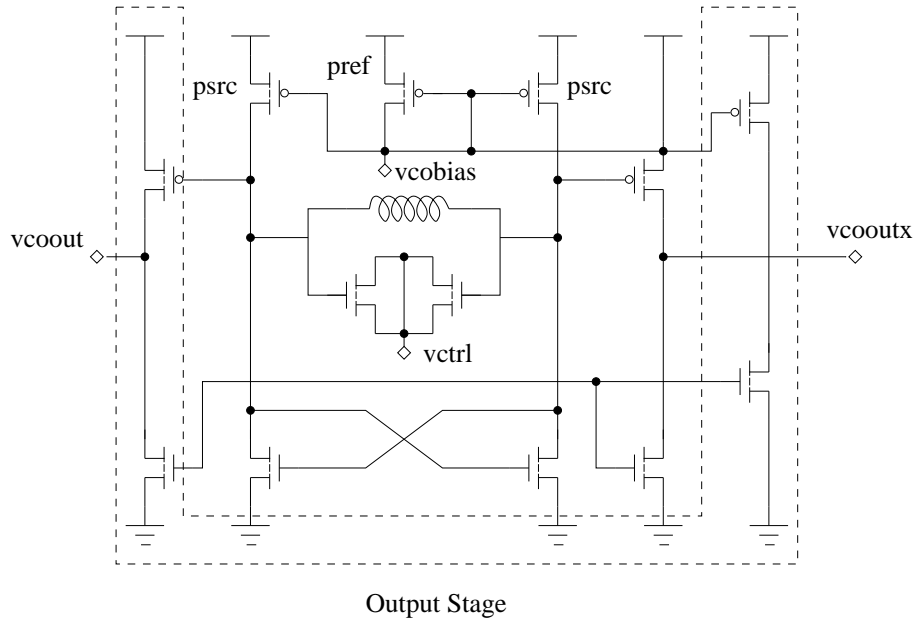
Figure 3.30: LC-VCO Block.
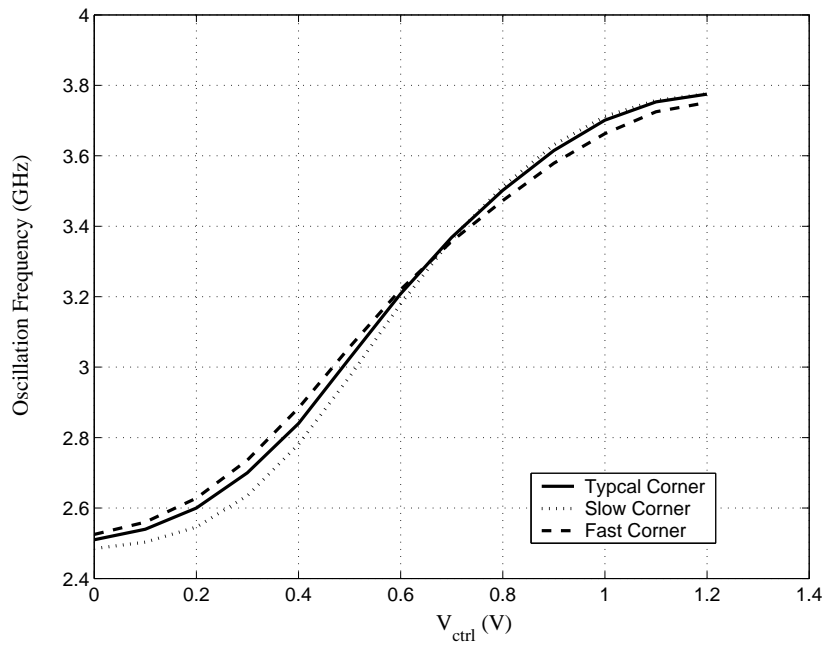
Figure 3.31: VCO tuning range.

design is to ensure that the flip-flop in the first stage responds fast enough to work with the PLL clock output. From extracted simulation, the clock divider can work up to $4GHz$ in all process corners.
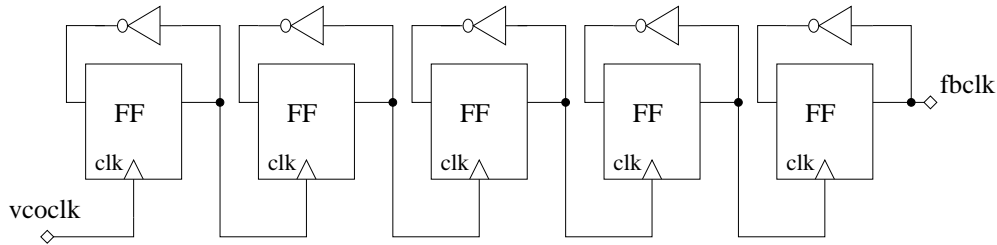
Figure 3.32: The schematic of the clock divider.

The PLL clock output is gated by an external clock enable signal *clken* (refer to Figure 3.28). The asynchronous enable block retimes the signal *clken* internally to ensure that a glitchless clock cycle is sent to the transmitter digital block when the clock signals are enabled. The schematic of the asynchronous enable block is illustrated in Figure 3.33.
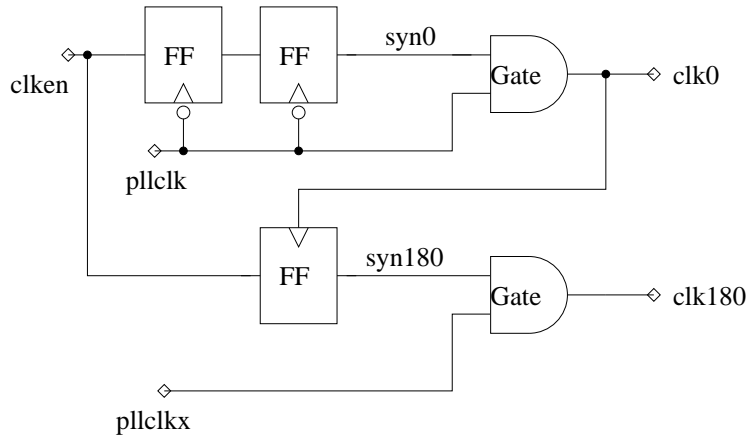
Figure 3.33: The schematic of the asynchronous enable block.

The asynchronous enable block uses two negative-edge triggered flip-flops to retime the signal *clken*. The output of the flip-flops *syn0* becomes the internal enable signal for the clock *clk*. Since the flip-flop is negative-edge triggered, it guarantees that signal *syn0* is high before the clock cycle begins. Thus, it ensures that the first clock pulse sent to the transmitter digital block is a full clock cycle.

To ensure that $clk0$ is leading $clk180$, $clk0$ is used to generate the internal enable signal for $clk180$. In Figure 3.33, the internal enable signal for $clk180$ is $syn180$. The timing of these signals is shown in Figure 3.34. Signal $syn0$ goes high after two negative edges of $pllclk$, and signal $syn180$ enables $clk180$ after $clk0$ goes high.
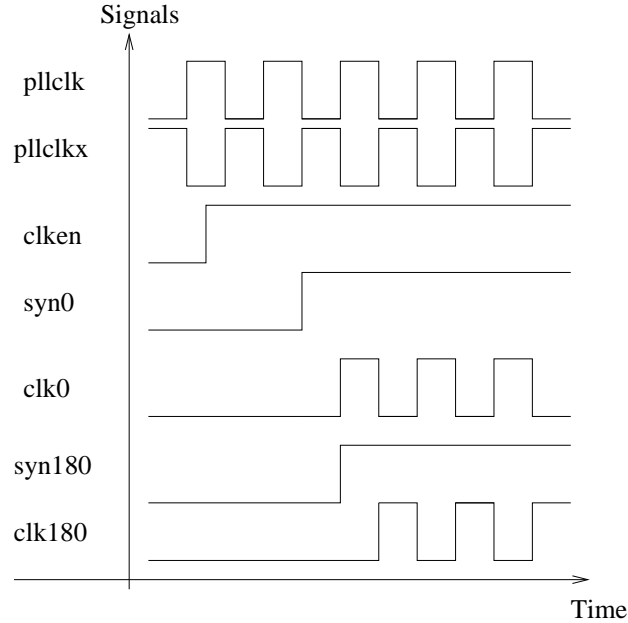
Figure 3.34: The asynchronous enable block circuit timing diagram.

3.5.1 PLL Layout

The $3GHz$ PLL layout in the transmitter testchip is shown in Figure 3.35. The size of the layout is $250\mu m \times 300\mu m$. The LC-VCO is drawn with perfect symmetry to ensure the differential output of the VCO is balanced. As expected, the layout of the inductor and the loop filter occupied most of the area. In addition, the inductor is placed $20\mu m$ from other circuits to minimize coupling.

3.6 Primitive Circuits

This section presents the implementation of the primitive circuits in the transmitter. Three main primitive circuits are used in the design: the sense-amplifier flip-flop, the
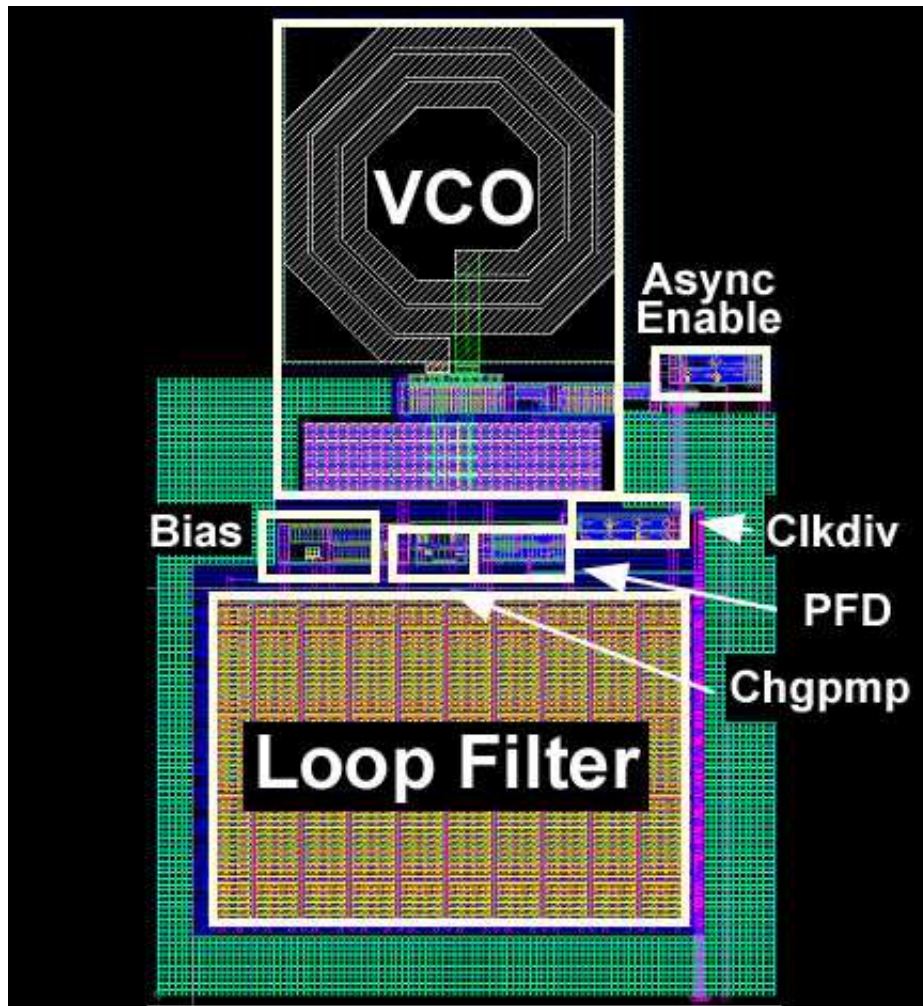
Figure 3.35: $3GHz$ PLL layout.

sense-amplifier multiplexor flip-flop, and the 2-to-1 multiplexor. The design and implementation of these circuits are presented in the following sections.

3.6.1 Sense-Amplifier Flip-Flop

The timing of the digital data in the transmitter is synchronized by a $3GHz$ clock. Due to the high-speed operation, conventional master-slave flip-flops cannot meet the timing requirements. As a result, the sense-amplifier flip-flop in Figure 3.36 is selected because of its ability to work with high-speed signals [NSO99].

The operation of the flip-flop is divided into two phases: the reset phase and the latch
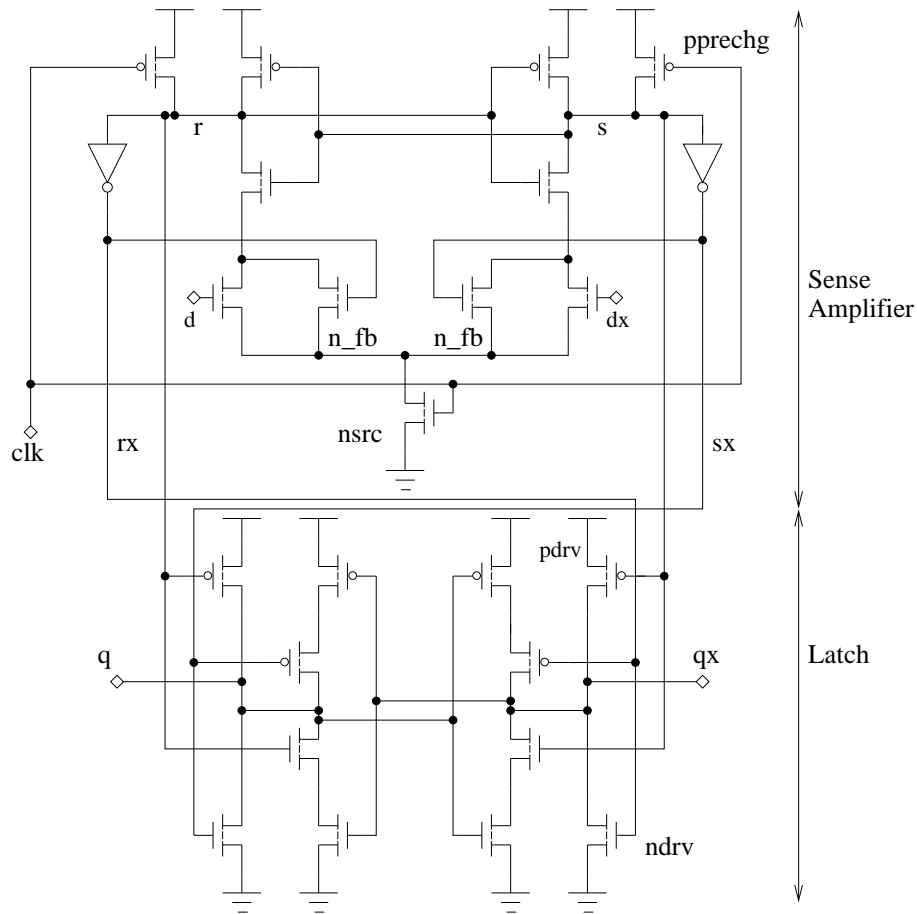
Figure 3.36: The sense-amplifier flip-flop.

phase. The flip-flop goes into the reset phase when clk is low and into the latch phase when clk is high. In the reset phase, the sense-amplifier is pre-charged, and any change from the flip-flop inputs, d and dx, is isolated from the flip-flop outputs, q and qx. At the same time, the latch retains the result from the previous latch phase and drives the flip-flop outputs. In the latch phase, the sense-amplifier amplifies the difference between the differential inputs d and dx. The result is written into the latch to drive the flip-flop outputs.

The sense-amplifier flip-flop has a clk-q delay of $90ps$. The output latch is designed to charge an output load of $36fF$, assuming a fan-out of four. The clock input capacitance is $9fF$, while the hold time of the flip-flop is $15ps$. The sense-amplifier flip-flop requires only a single phase clock. This reduces the clock loading of the transmitter, and ease

the clock signals routing.

3.6.2 Sense-Amplifier Multiplexor Flip-Flop

The sense-amplifier multiplexor flip-flop has the same structure as the sense-amplifier flip-flop described in Section 3.6.1. However, there is a 2-to-1 multiplexor built into the input stage of the sense-amplifier, which is equilvalent to a 2-to-1 multiplexor cascaded in front of a sense-amplifier flip-flop. The schematic is shown in Figure 3.37.
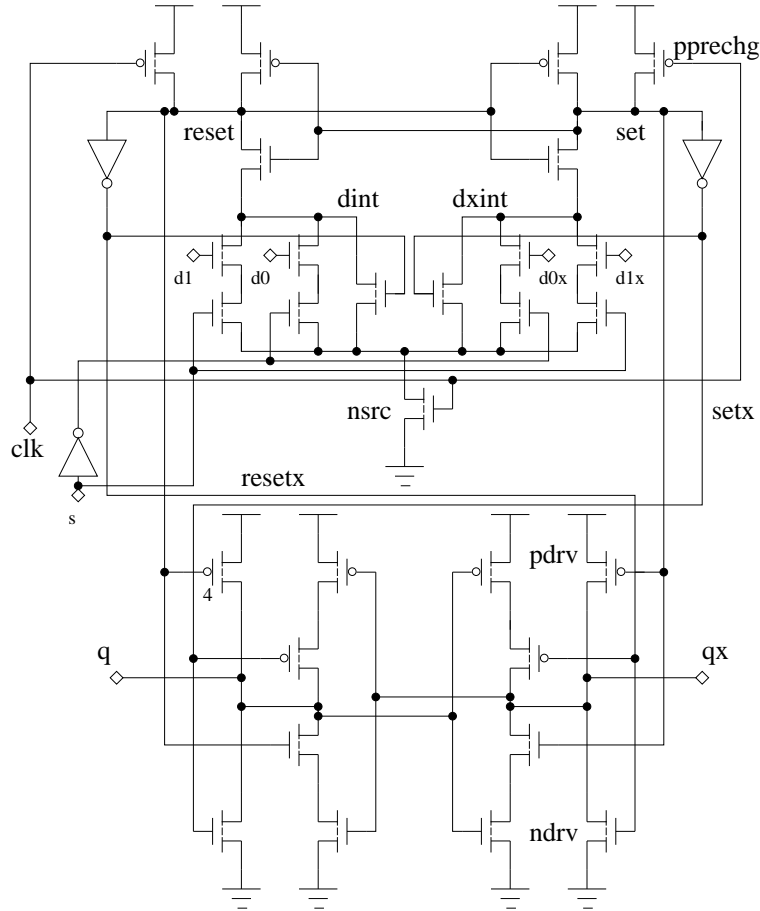
Figure 3.37: The combined 2-to-1 multiplexor and sense-amplifier flip-flop.

The select input *s* multiplexes the input data into the sense-amplifier. It selects either *d0* and *d0x* or *d1* and *d1x* as the inputs to the sense-amplifier. The internal capacitance at nodes *dint* and *dxint* of the sense-amplifier is larger due to the connection of two extra NMOS transistors. As a result, the clk-q delay is 110*ps*, slightly larger than the original

sense-amplifier flip-flop. Although the sense-amplifier multiplexor flip-flop suffers a slight penalty in the clk-q delay, it still operates faster than cascading a 2-to-1 multiplexor in front of a sense-amplifier flip-flop. The loading for the clock and data inputs are kept to the same values, $9fF$ and $3fF$ respectively.

3.6.3 High-speed Digital 2-to-1 Multiplexor

The multiplexor circuit used throughout the chip is shown in Figure 3.38 [Rab96]. Input s selects either a or b to the output of the multiplexor. This is a high-speed multiplexor compared to the traditional AND-OR gate multiplexor because it only has one gate delay plus buffering. The input to output delay of the multiplexor is $120ps$. The output of the multiplexor is designed to drive a capacitive load of $17fF$, assuming a fan-out of four.
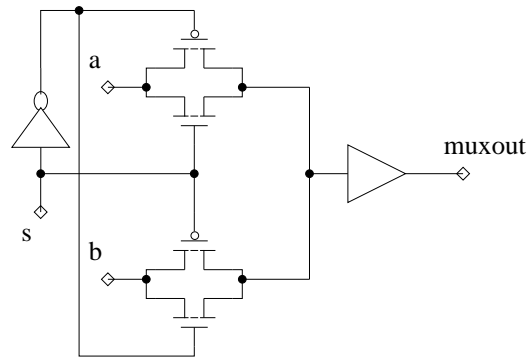
Figure 3.38: The high-speed 2-to-1 multiplexor.

3.7 Summary

This chapter covers the transmitter architecture and the approach used for reflection cancellation. It further describes the circuits that are used in the design of the transmitter as well as the why the design choices are made. The transmitter digital block generates and processes the data, and the transmitter front-end sends out the data to the channel. The mini-JTAG controller and the scan-chain in the transmitter provide a convenient way to input the parameters required by the cancellation processes. The

PLL that is used as a clock generator is covered in detail. The PLL provides a differential $3GHz$ clock output for the transmitter. Finally, the primitive circuits such as the sense-amplifier flip-flop and 2-to-1 multiplexor are described. The following chapter presents the system operation modes and the simulation results.

4 System Operation Modes and Simulation Results

This chapter discusses the transmitter operation modes and the system simulation results. Before data transmission, the channel characteristics must be obtained. From the channel characteristics, the ISI and reflection-cancellation parameters need to be adjusted properly. The process of obtaining the channel characteristics, adjusting the parameters, and transmitting data are done in different operation modes. The simulation results presented in the chapter show the effectiveness of the reflection and ISI cancellation through the use of eye diagrams.

4.1 System Operation Modes

There are three different operation modes in the transmitter: the scan-in mode, the calibration mode, and the data transmission mode. The scan-in mode loads the transmitter scan-chain with the scan-in data sequence. The calibration mode sends out the calibration sequence to obtain the channel characteristics. Finally, the data transmission mode sends the data to the channel. The details of these operation modes are explained in the following.

4.1.1 Scan-in Mode

In the scan-in mode, the transmitter loads in a 360-bit data sequence for the scan-chain. This includes the initial sequence for the data generator (256 bits), the control bits for the variable delay block (12 bits), the control bits for the bit inversion block (24 bits), the control bits for the amplitude of the pre-emphasis and the reflection-cancellation drivers (66 bits), and the control bits for the operation modes (2 bits). During the scan-in mode, the PLL output is disabled until the data sequence is loaded into the scan-chain.

The functionality of the mini-JTAG controller is simulated with Hsim. The simulation begins with the mini-JTAG controller in the reset state. The *tms* signal is given an input sequence of [0100] to bring the controller state to "ShDR" as shown in Figure 4.1. The controller FSM diagram was discussed in Section 3.3.6. The scan-in process starts in the "ShDR" state by enabling the scan-clock *sclk* with the *sen* signal. The scan-clock runs at $83MHz$ and it takes $4.3\mu s$ to completely scan the 360-bit data sequence into the scan-chain. At the end of the scan-in process, the mini-JTAG controller is returned to the idle state "RTI".
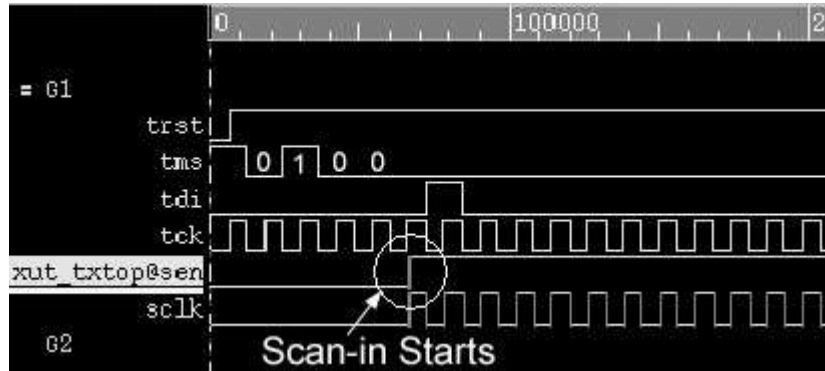
Figure 4.1: Scan-in operation.

4.1.2 Calibration Mode

The calibration mode is used to measure the channel characteristics and allows users to adjust the parameters of the pre-emphasis and reflection canceller. To measure the channel characteristics, the transmitter repeatedly sends out a calibration sequence on the channel. From the calibration sequence, the parameters are adjusted accordingly based on the results at the receiver, an oscilloscope. To change a parameter, the transmitter has to revert back to the scan-in mode and rescan all the parameters into the scan-chain with updated values.

The channel characteristics are obtained with the method described previously in Section 2.2.1. This method requires a special symbol, the zero symbol, to be sent out. The implementation of the zero symbol was discussed in Section 3.4.1. The normal symbols in a differential transmission are '1' and '-1'. The calibration sequence is 128-bit in length, which has a '1' symbol in the midst of '-1' symbols. During the calibration

mode, the transmitter front-end converts all the '-1' symbols into zero symbols.

Using this method, the amount of ISI is determined by directly observing the output waveform. By adjusting the amplitude of the pre-emphasis taps, ISI with up to 3UI duration can be cancelled. The amount of signal reflection is determined also by observing the output waveform. The coefficients of the 8-tap reflection canceller are adjusted such that the reflections are completely removed or are zeroed out in the middle of the unit interval. The timing of the reflection-cancellation signal is adjusted by setting the 6-bit variable delay control. The timing of the 8-tap is adjusted such that it covers the entire duration of the reflection. If that is not possible, the taps are adjusted to eliminate the most dominant reflection. The simulation result of the calibration mode is shown along with the result of the reflection and ISI cancellation later in this chapter.

4.1.3 Data Transmission Mode

Data transmission begins after calibration is completed. The transmitter is able to transmit two different sequences of data: the $2^{31} - 1$ bit PRBS and the 128-bit user-defined sequence. Their initial values are loaded into the data generator during the scan-in mode. The simulation result of the data transmission is shown as received signal eye diagrams later in this chapter.

4.2 Simulation Results

The extracted netlist of the transmitter is simulated in Hspice to demonstrate the capability of the reflection-cancellation circuitry. Two simulations, each with a different channel, are presented here: one has severe termination impedance mismatches, and the other includes two inductors. Also, simulations for ISI-cancellation are done separately by using a lossy channel. The received signal eye diagrams, before and after cancellation, are compared in all simulations.

4.2.1 Reflection Cancellation

The reflection-cancellation capability of the transmitter is demonstrated by simulating the transmitter with a channel that includes impedance mismatches. The transmitter is simulated in the calibration mode at 6Gbps to obtain the channel impulse response. The

channel, as shown in Figure 4.2, is $8cm$ long and is modelled with the T-model (lossless channel model) in Hspice. Lossless channel model is used so that only the effect of reflections is shown. To create impedance mismatches, the channel characteristic impedance is increased to 100Ω from the common value, 50Ω. The transmitter termination remains at 50Ω, but the receiver termination is reduced to 25Ω to create larger reflections. As a result, resistive reflections occur at both the transmitter and receiver sides.
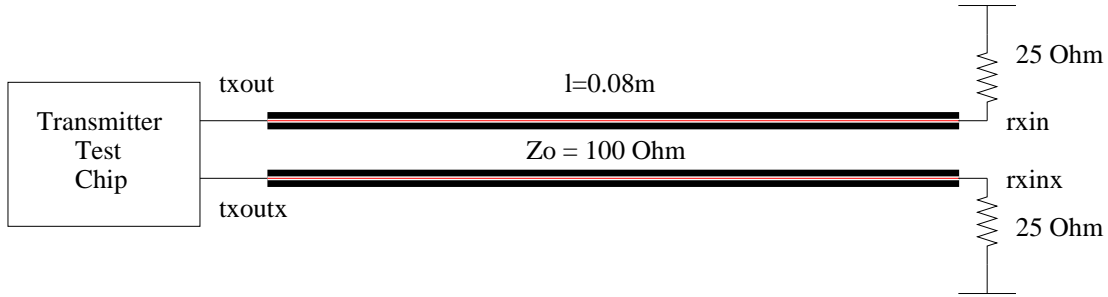
Figure 4.2: Channel with termination mismatches used in reflection cancellation simulation.

Hspice simulation of the impulse response before reflection cancellation is shown in Figure 4.3 as dashed line. The time scale of the plot is adjusted such that the received pulse starts at zero second. The amplitude of the received pulse is $90mV$. The first reflection arrives at the receiver after $1ns$ with an amplitude of $30mV$. Since the first reflection is not cancelled, it causes a second reflection, which arrives at the receiver with an amplitude of $11mV$ after $2ns$ of the received pulse.

The transmitter is switched to the data transmission mode to show the effect of the multiple reflections on the received signal. The quality of the received signal is illustrated with an eye diagram in Figure 4.4. The reflections cause the eye diagram to have a vertical opening of $70mV$ and a time jitter of $50ps$. The next simulation shows that the quality of the received signal is improved by enabling reflection cancellation in the transmitter.

The transmitter is returned to the calibration mode to adjust the reflection-cancellation signals. Since the first reflection occur after 6UI, the 6th reflection-cancellation driver is used with an amplitude of $-37.2mV$. The result is shown in Figure 4.3. The solid line shows the impulse response after reflection cancellation. The first reflection is reduced to $9mV$ from $30mV$. In addition, since the first reflection is reduced, the second reflection is lowered to $4mV$ from $11mV$. The following data transmission simulation illustrates
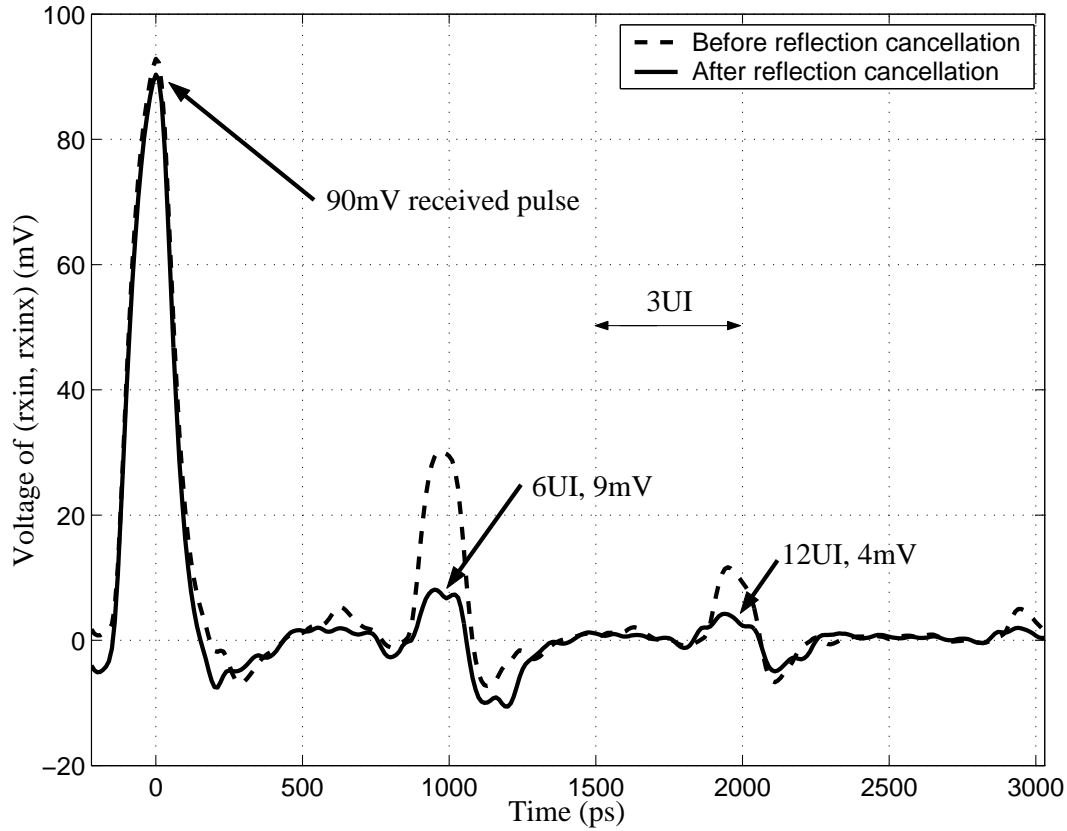
Figure 4.3: The channel impulse response before and after reflection cancellation.

that significant improvment is made in the eye diagram by using reflection cancellation.

The transmitter is simulated in the data transmission mode with reflection cancellation enabled. The received signal eye diagram is shown in Figure 4.5. It can be seen that the vertical eye opening is increased to $140mV$ from $70mV$, and the time jitter is lowered to $30ps$ from $50ps$ prior to reflection cancellation. This simulation shows that the transmitter is able to operate and produce relatively clean signal at the receiver under severe termination mismatched channels.

To further demonstrate the reflection cancellation capability of the transmitter, a channel with two impedance discontinuities is created. The channel, as shown in Figure 4.6, consists of three $4cm$ segments of a $12cm$ lossless transmission line and two $4nH$ inductors for creating impedance discontinuities. The size of the inductors is intentionally enlarged to worsen the reflections in the channel. Finally, the channel is properly terminated at both the transmitter and the receiver side with 50Ω resistors.
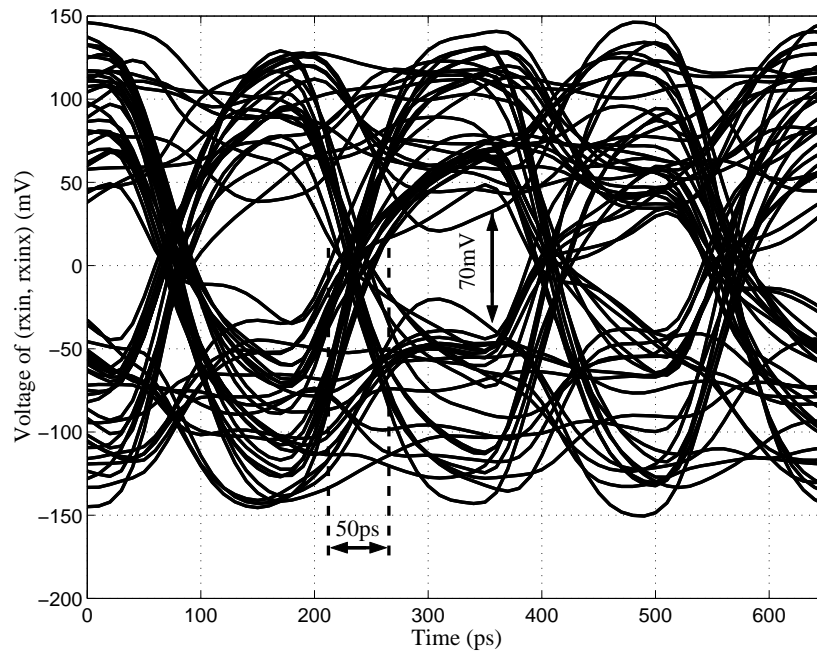
Figure 4.4: Received signal eye diagram before reflection cancellation.

Figure 4.5: Received signal eye diagram after reflection cancellation.
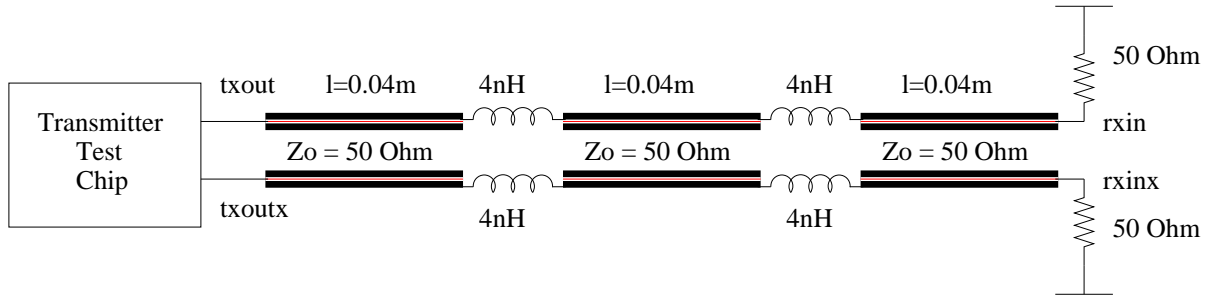
Figure 4.6: Channel with impedance discontinuities used in reflection cancellation simulation.

Initially, the transmitter sends the calibration sequence on the channel with both the pre-emphasis drivers and the reflection-cancellation drivers disabled. The received signal before reflection cancellation is shown in Figure 4.7 as dashed line. The time axis is scaled such that the received pulse starts at zero second. As expected, one inductive reflection goes back to the receiver and arrives $500ps$ after the received pulse. This reflection, if not cancelled, causes signal detection errors.

To show how the received signal is affected by the reflection, the transmitter is simulated in the data transmission mode. The transmitted data is sent to the channel at 6Gbps with an amplitude of $400mV$. The eye diagram of the received signal presented in Figure 4.8 shows the effect of the reflections. Signal reflections interfere with the received signal and cause the eye diagram to have $80mV$ of vertical eye opening and $100ps$ of time jitter.

The eye diagram can be improved by reducing the reflections that travel back to the receiver. With the transmitter operating in the calibration mode, the calibration sequence is sent to the channel. The inductive reflection has a positive portion that occurs at $600ps$ and a negative portion at $700ps$ as shown in Figure 4.7. The positive portion occurs approximately 4UI after the main received pulse so the 4th reflection-cancellation driver is used with an amplitude of $-37.2mV$. For the negative portion of the inductive reflection, the 5th reflection-cancellation driver is used with an amplitude of $27.9mV$. By tuning the two reflection-cancellation drivers, the optimal result of the calibration is shown in Figure 4.7. Since the reflections do not occur in the middle of the unit interval, they cannot be fully cancelled. The positive portion is reduced from $42mV$ to $19mV$, and the negative portion is lowered from $-30mV$ to $-21mV$.
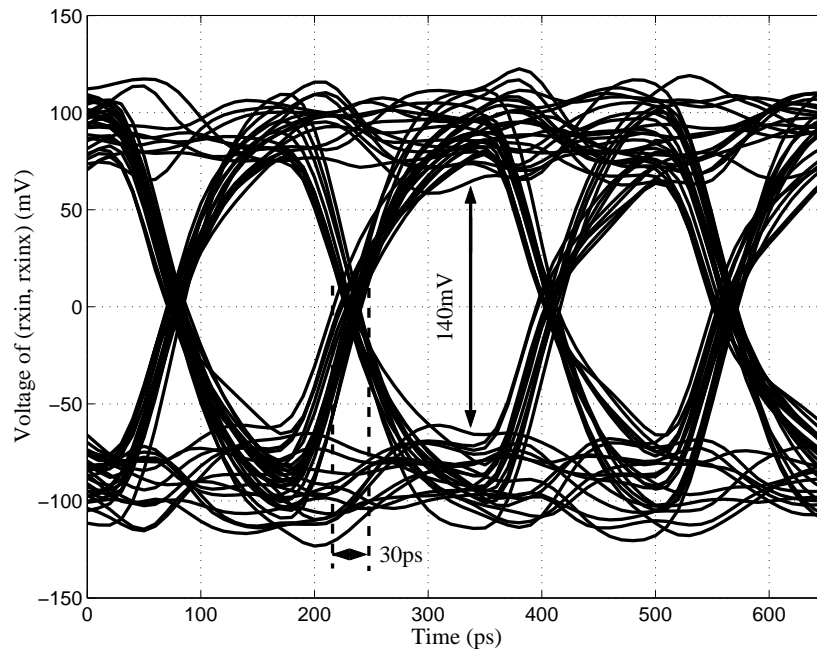
After the calibration, the transmitter is switched back to the data transmission mode.
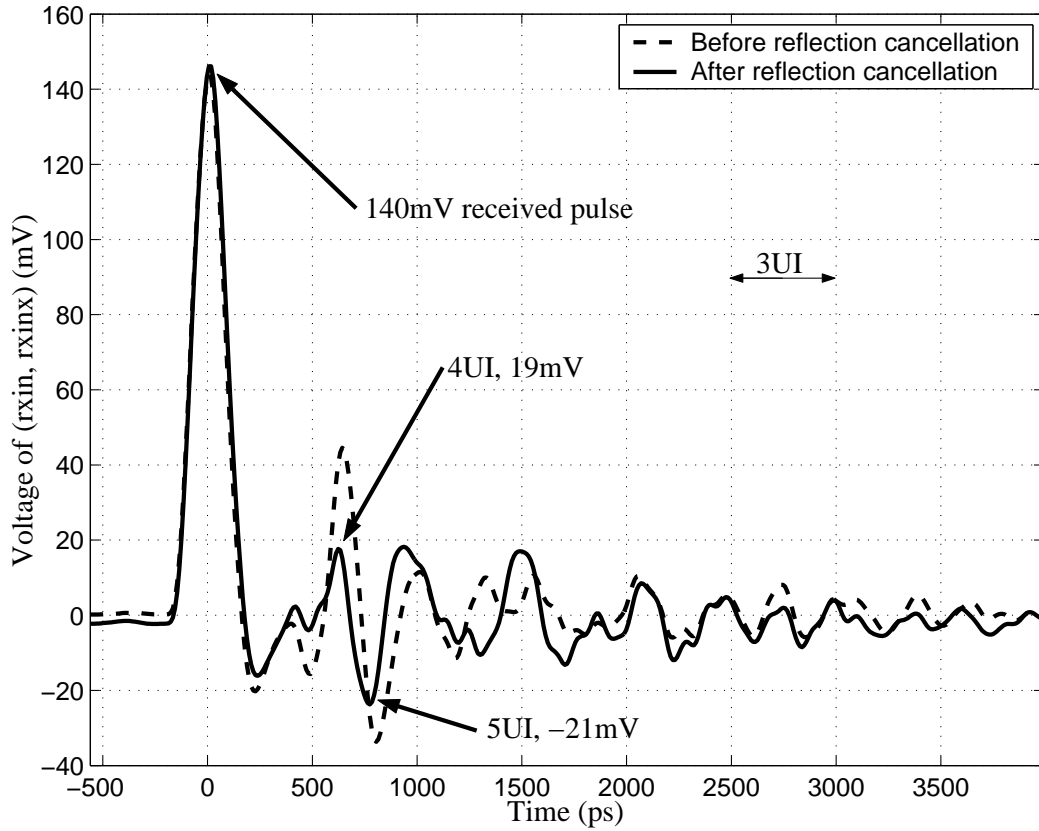
Figure 4.7: The channel impulse response before and after reflection cancellation.

The received signal eye diagram is shown in Figure 4.9. The eye diagram shows larger eye openings than the one without reflection cancellation. The vertical eye opening has increased to $160mV$ and the time jitter has decreased to $75ps$. As a result, the reflection-cancellation scheme improves the signal quality at the receiver by having larger received signal amplitude and reduced time jitter.

4.2.2 ISI Cancellation

The ISI cancellation capability of the transmitter is demonstrated by simulating the transmitter with the low-pass channel as shown in Figure 4.10. The low-pass characteristic of the channel is represented by the first order RC filter with a -3dB frequency of $2.1GHz$ such that adequate ISI is produced. The pair of 50Ω resistors are used for termination to provide a 25Ω loading at the transmitter outputs. The ideal buffer is
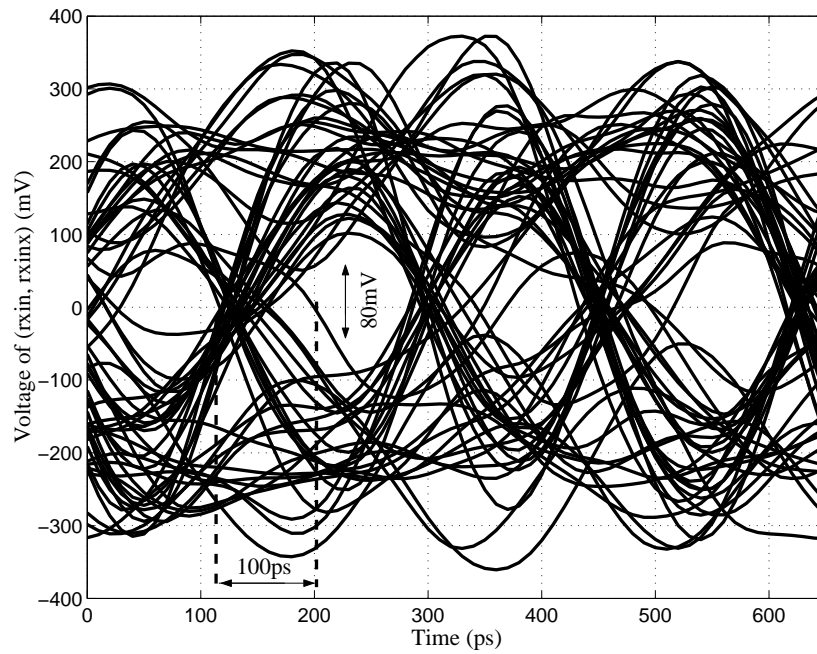
Figure 4.8: Received signal eye diagram before reflection cancellation.
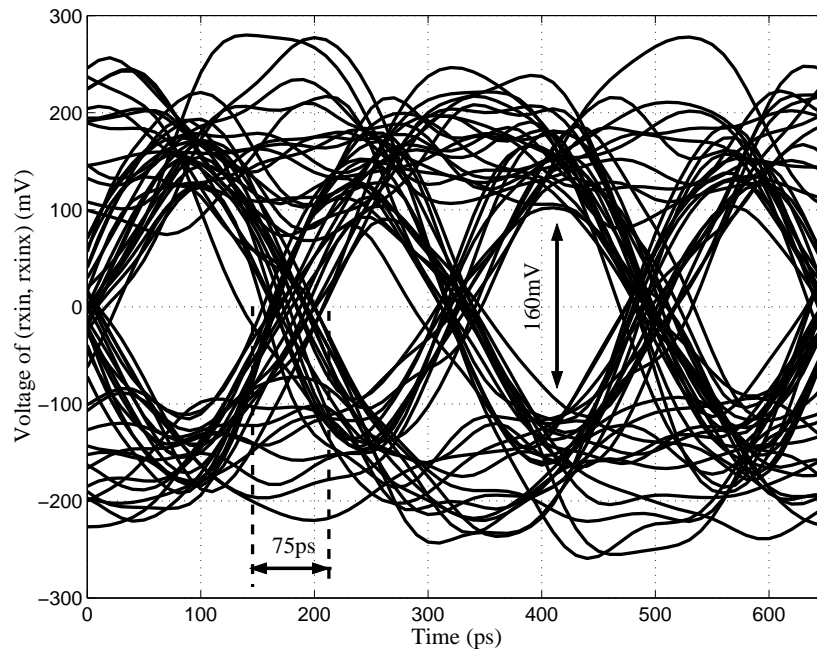
Figure 4.9: Received signal eye diagram after reflection cancellation.

used to separate the transmitter with the channel output. This setup is similar to a simulation with the transmitter and a Hspice W-element model; however, the simulation time is shortened since the signal propagation time is ignored.
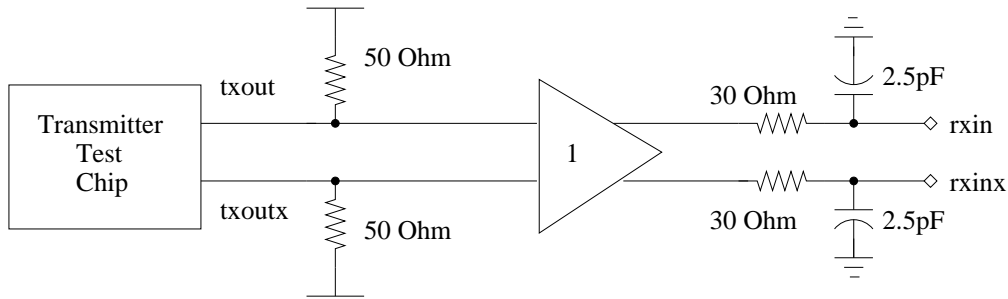
Figure 4.10: Channel model used in ISI cancellation simulation.

To obtain the channel impulse response, the transmitter sends the calibration sequence on the channel. The received pulse before ISI cancellation is shown in Figure 4.11 as dashed line. The time axis is shifted such that the received pulse starts at zero seconds. The received signal has an amplitude of $140mV$, which is attenuated from a $200mV$ transmitted pulse. The tail of the received signal extends until $500ps$, and it causes a $30mV$ ISI after one unit interval.

The transmitter is then simulated in the data transmission mode with ISI cancellation disabled. The received signal eye diagram is shown in Figure 4.12. The eye diagram has a vertical opening of $200mV$ and a time jitter of $25ps$. ISI cancellation can help to enlarge the eye opening by lowering the amplitude of the transmitted signal and emphasizing the signal transitions.

The transmitter is switched back to the calibration mode to find the optimal amplitude of the pre-emphasis signals for ISI cancellation. Simulation shows that the optimal received signal results when the amplitude of the first pre-emphasis driver is set to $-47.55mV$. Figure 4.11 shows the impulse response of the channel after ISI cancellation. The ISI after one unit interval is reduced to less than $10mV$.

To show the improvment of the ISI cancellation on the received signal, the transmitter is simulated in the data transmission mode with the pre-emphasis driver enabled. Figure 4.13 shows the eye diagram of the received signal, which has an eye opening of $300mV$ and a time jitter of less than $25ps$, compared to $200mV$ and $25ps$ respectively prior to ISI cancellation. This shows that ISI cancellation has improved the eye opening of the
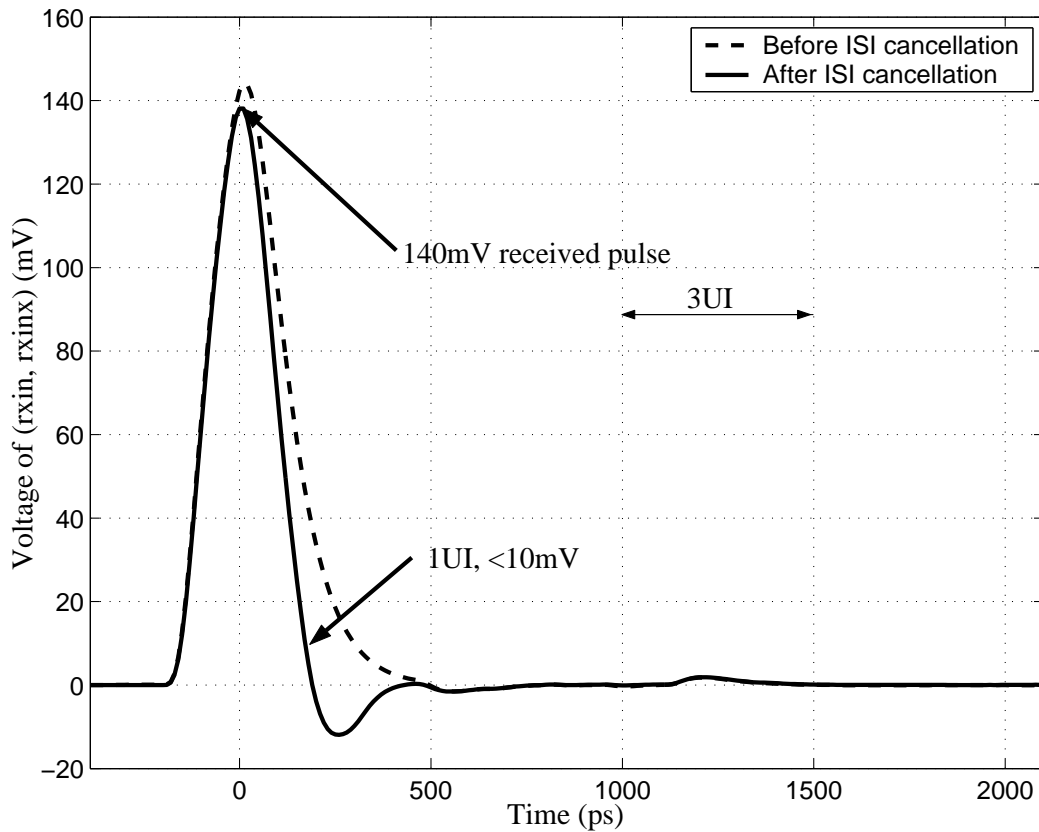
Figure 4.11: The channel impulse response before and after ISI cancellation.

received signal.

4.2.3 Power Consumption

The power consumption of the transmitter, excluding the PLL, is simulated to be $297.3mW$ per channel in the typical condition. The contribution of each circuit block to the total power consumption is shown in Figure 4.14. More than half of the transmitter power (55%) is comsumed in the data generator due to the use of a large number of flip-flops (256 in total). The variable delay block consumes $81mW$ (27%) from the flip-flops (128 in total) used to delay the transmitted data. The rest of the circuits in the digital block and the transmitter front-end contribute 16% to the total transmitter power consumption. The power consumption of the pre-emphasis driver and the reflection cancellation driver is assumed to have a combined tail current of $5.25mA$, which is
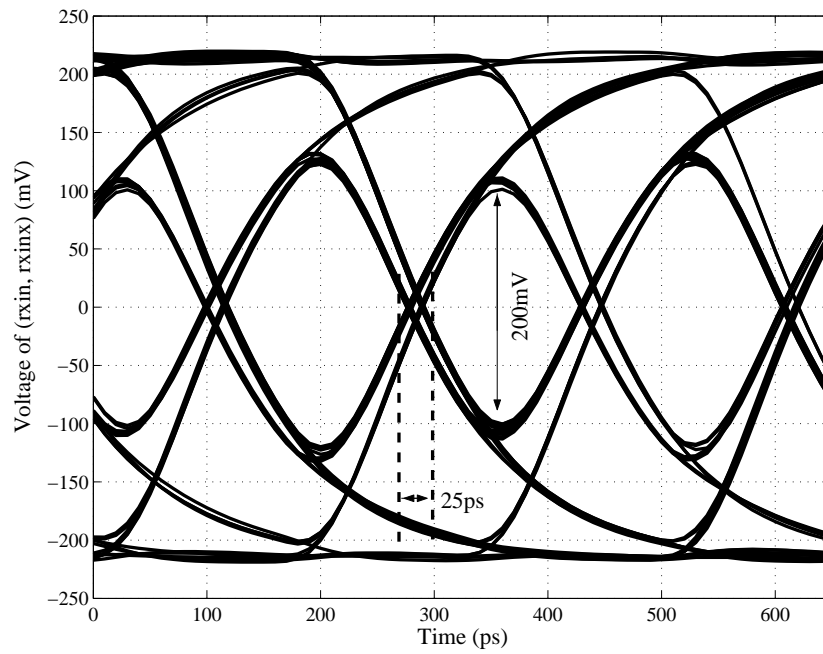
Figure 4.12: Received signal eye diagram before ISI cancellation.
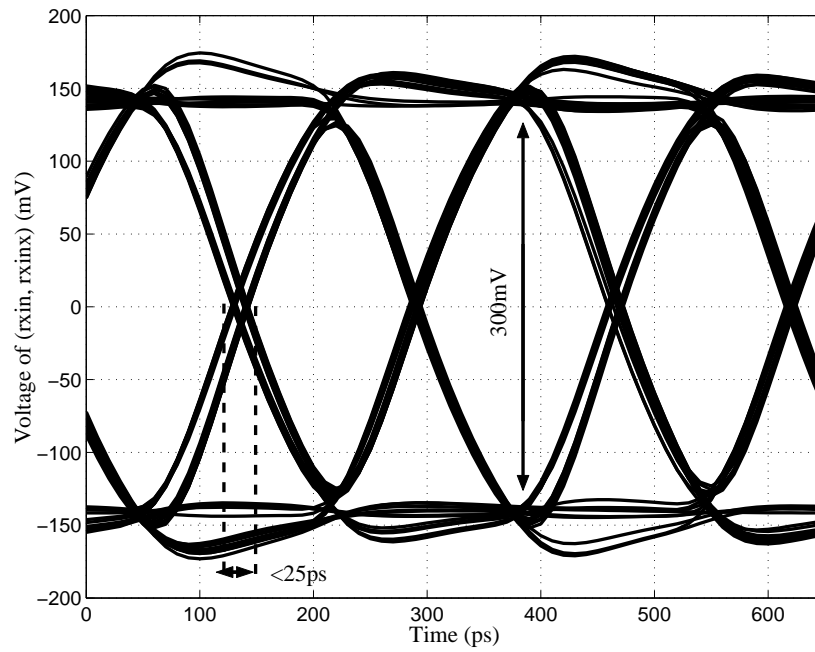
Figure 4.13: Received signal eye diagram after ISI cancellation.

the amount of current used to cancel the reflection in the channel as shown previously in Figure 4.10.

Data Generator	Variable Delay Block	Rest of Digital Block	Driver+Bias	Data Multiplexors	Pre–emphasis & Reflection Canceller
163mW (55%)	81mW (27%)	27mW (9.1%)			

10mW (3.4%) 10mW (3.4%) 6.3mW (2.1%)
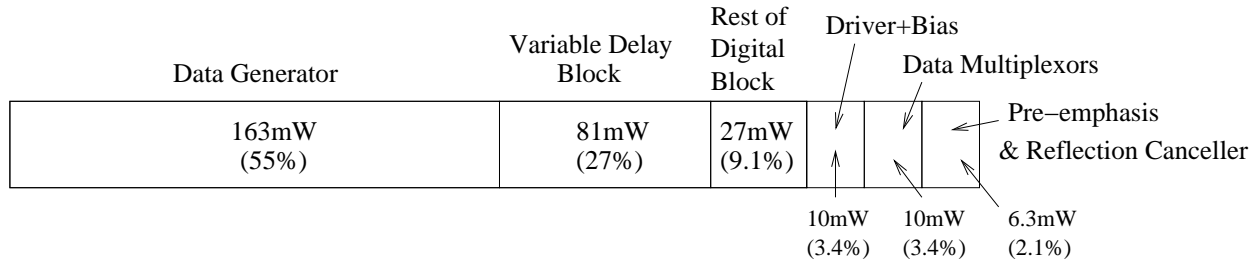
Figure 4.14: Contributions of the transmitter power consumption.

In a production chip, the data generator is not needed, and hence its power consumption should not be included when measuring the total power consumption. Thus, the estimated power consumption in a production chip is only $134mW$ per channel.

4.3 PLL Simulation

The extracted netlist of the $3GHz$ PLL is simulated for lock acquisition and phase noise. Lock acquisition simulation ensures that the PLL is able to acquire phase and frequency locking between the frequency-divided VCO clock and the external reference clock. With the control voltage initialized to $0V$, the PLL is simulated until the VCO control voltage reaches a stable value to ensure phase and frequency locking. Phase noise simulation is then done to measure how the noise that is generated by the PLL components and the reference clock affects the PLL output. From the PLL phase noise plot, the Root Mean Square (RMS) jitter of the PLL is measured.

4.3.1 PLL Lock Acquistion

To ensure that the PLL is able to obtain locking after it starts up, a transient simulation is done on the PLL with the VCO control voltage initialized to $0V$ and the reference clock set to $93.75MHz$. The transient waveform of the VCO control voltage is shown in Figure 4.15. The PLL obtains locking after $1.8\mu s$ with the final VCO control voltage stabilizing at $540mV$, which produces an output clock frequency of $3GHz$. Near lock,

the Hspice output exhibits no ringing which illustrates that the damping factor ζ is correctly designed.
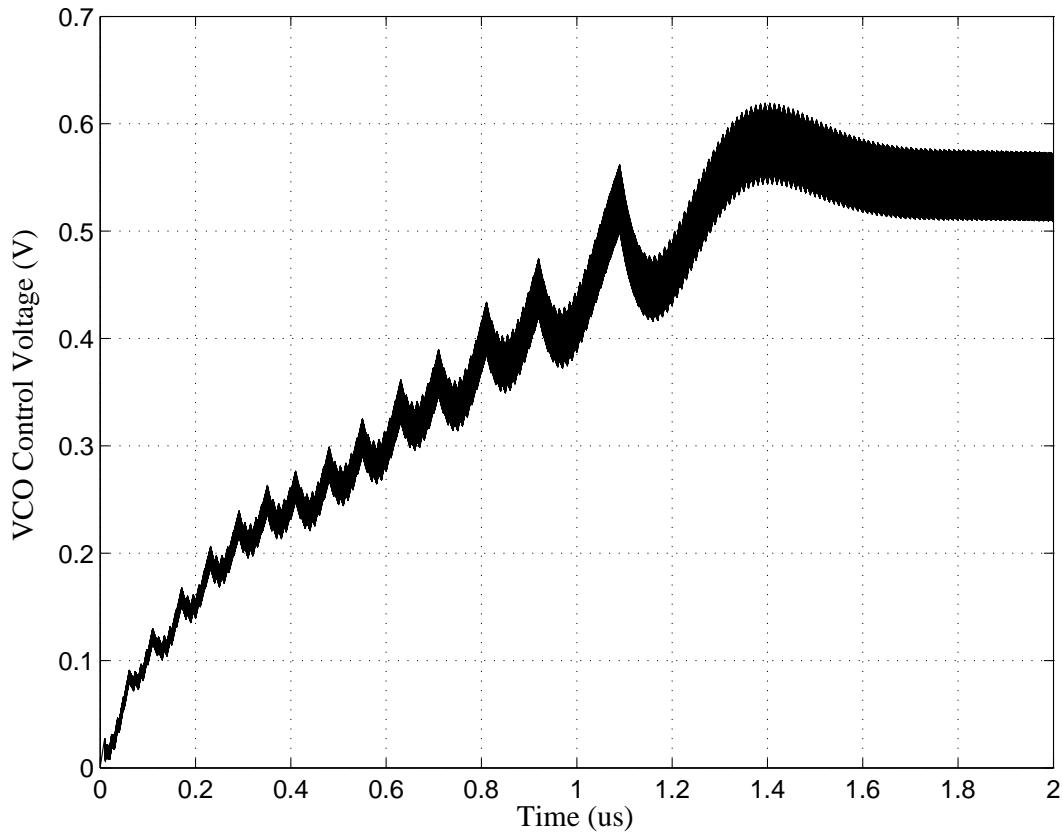
Figure 4.15: PLL lock acquisition.

4.3.2 Phase Noise

The phase noise of the PLL is simulated with Fujitsu's in-house tool and is shown in Figure 4.16. The simulation result includes both white noise and 1/f noise. The phase noise at $100kHz$ offset is $-90dBc/Hz$. To find out the RMS jitter of the PLL, the phase noise plot is integrated. The RMS jitter is measured to be $17ps$, which gives a peak-to-peak jitter of $102ps$.
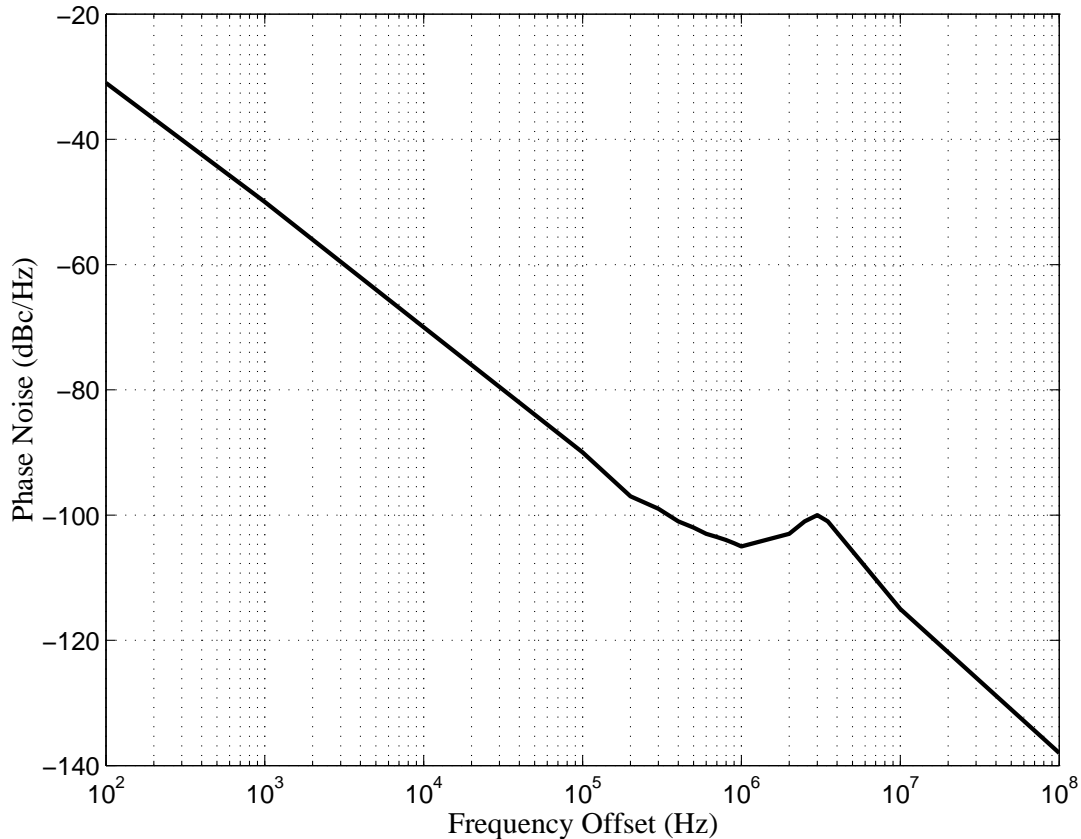
Figure 4.16: PLL phase noise plot.

4.4 Transmitter Testchip Layout and Specifications

The top level layout of the transmitter testchip is shown in Figure 4.17. The transmitter has an active area of $800\mu m \times 430\mu m$ and is placed in the middle top side of the testchip to minimize the length of the bondwire needed. The chip is implemented in Fujitsu's $0.11\mu m$ process and is currently under fabrication.

The specification of the transmitter testchip is summarized in Table 4.1. The transmitter has a two-way interleaving structure yielding a differential data rate of 6Gbps. The two data blocks operating concurrently, each require a $3GHz$ clock. The 3Gbps data streams from the data blocks are combined into a 6Gbps data stream for the drivers. With a $1.2V$ DC supply, the transmitter consumes $297mW$ of power.

The data driver sinks $8mA$ of current and produces a $200mV$ swing on a 50Ω channel. For ISI equalization, a 3-tap pre-emphasis driver is used. In addition, an 8-tap reflection-

72
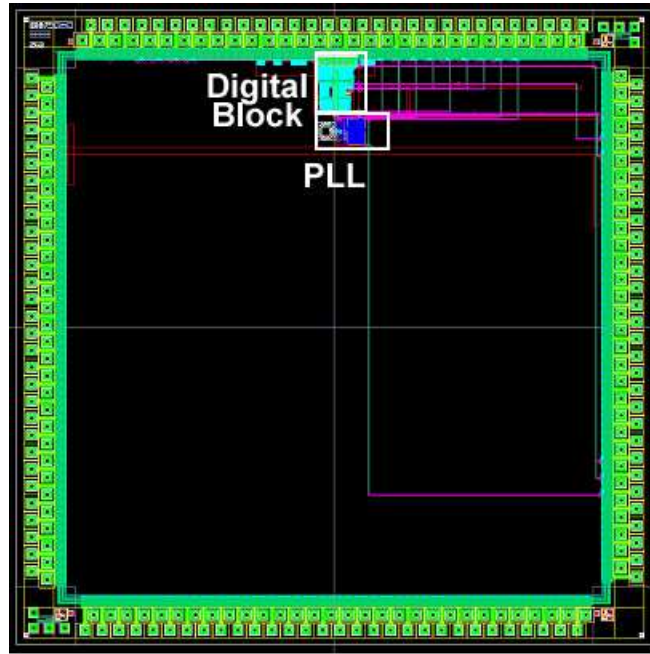
Figure 4.17: Testchip layout.

cancellation driver removes the signal reflections that are caused by channel impedance discontinuities. The 8 continuous taps can be delayed from 0 to 126 UIs to match the timing of the reflections. The ISI and reflection-cancellation drivers use similar driver implementations as the data driver. There is a 6-bit control for the current source in each tap, which can sink a maximum of $8mA$.

The chip has an integrated $3GHz$ PLL to provide the clock for the transmitter. The PLL requires an external reference clock between the range of $78.125MHz$ and $118.75MHz$ to generate an output clock frequency between $2.5GHz$ and $3.8GHz$. The testchip also supports an external clock to bypass the PLL clock. It is estimated that the highest input frequency for the bypass clock is $200MHz$.

4.5 Summary

This chapter presents the transmitter operation modes and the transmitter simulation result. There are three operation modes for the transmitter: the scan-in mode, the calibration mode, and the data transmission mode. Scan-in mode allows the parameters

Table 4.1: Transmitter testchip specifications.

Name	Symbol	Value			Units	Notes
		Min	Typ	Max		
Technology			0.11		μm	
Power Supply		1.14	1.20	1.26	Volts	
Reference Clock Frequency	f_{ref}	78.125	100	118.75	MHz	
PLL Clock Frequency	f_{clk}	2.5	3	3.8	GHz	
Data Rate				6	Gbps	
Signal Swing	V_{sw}		200		mV	
Pre-emphasis	$V_{preemph}$	-200		200	mV	7-bit
Reflection Cancellation	V_{cancel}	-200		200	mV	7-bit
Power Consumption	P		297		mW	
Layout Size			800×300		μm^2	

to be scanned into the scan-chain of the transmitter. The calibration mode obtains the channel characteristics and allows the adjustment of the pre-emphasis and reflection-cancellation drivers. The data transmission mode sends the transmitted data to the channel. The simulation result from Hsim shows that the mini-JTAG controller is able to start the scan-in process by enabling the scan-clock at the correct FSM state. Hspice simulation results illustrate that improvments are made on the received signal eye diagrams by using the ISI and reflection-cancellation scheme. Finally, Hspice simulation results show that the PLL is functional and is able to obtain phase locking during operation.

5 Conclusions

5.1 Summary

This thesis presented the design and implementation of a 6Gbps transmitter with ISI
and reflection cancellation. The transmitter can be divided into three main sections: the
transmitter digital block, the transmitter front-end and the PLL block. The transmitter
has a 2-way interleaving architecture, in which two half-rate data streams are combined
into one. The transmitter digital block provides the two half-rate data streams from
the $2^{31} - 1$ PRBS generator or the 128-bit user-defined data sequence. The transmitted
data is retimed and, if necessary, inverted before passed to the transmitter front-end for
transmission.

The transmitter front-end includes the high-speed data multiplexors, the data driver,
the pre-emphasis drivers, the reflection-cancellation drivers, the bias circuits, and the
termination resistors. The data multiplexors merge the two 3Gbps data streams from
the transmitter digital block into a 6Gbps data stream. The data driver then sends out
the combined data stream onto the channel. The ISI and reflection-cancellation drivers
use the delayed version of the transmitted data to cancel the ISI and reflections on the
channel.

ISI is cancelled by a 3-tap pre-emphasis driver in the transmitter. By adjusting the
6-bit digital control for each of the three pre-emphasis drivers, up to three UI of ISI
can be cancelled. Reflections are cancelled by an 8-tap reflection canceller that is also
implemented in the transmitter. The 6-bit variable delay block is used to delay the
cancellation signals to match the timing of the reflections. A maximum delay of 126UI,
with 1UI resolution, is possible from the variable delay block. The amplitude of the taps
can be individually adjusted to match the shape of the reflections. For the reflections
that are not located in the middle of the unit interval, the cancellation signals are
adjusted such that the reflections located at the interval boundaries are reduced as
much as possible, while emphasizing on zeroing the reflections in the middle of the unit

intervals.

The $3GHz$ PLL is used as a clock generator for the transmitter. The PLL uses an LC-VCO as the oscillator, which has a tuning range between $2.5GHz$ and $3.8GHz$. There is an optional bypass clock to serve as a backup if the PLL malfunctions.

A testchip of the transmitter is implemented with the Fujitsu's $0.11\mu m$ CMOS process Extensive post-layout simulation is done on the transmitter to verify its functionality. Simulation shows that improvments are made on the received signal eye diagram when reflections and ISI are cancelled. The PLL has an acquistion time of less than $2us$. In addition, the phase noise at $10kHz$ offset is $-90dBc/Hz$, and it has an RMS jitter of $17ps$.

5.2 Contributions

The transmitter described in the thesis is designed for chip-to-chip signaling applications. The transmitter is capable of transmitting data at 6Gbps. It has a 3-tap pre-emphasis driver for ISI equalization and an 8-tap reflection canceller for canceling signal reflections in the channel.

A testchip of the transmitter is implemented in Fujitsu's $0.11\mu m$ CMOS process, and has been submitted for fabrication. Simulation results including severe impedance mismatch and inductive reflections verify the testchip functionality at 6Gbps.

5.3 Future Work

There are four main areas in the transmitter design that can be considered for future work: the time resolution of the reflection-cancellation block, the flexibility of the reflection-cancellation taps, the automatic adjustment of the cancellation parameters, and the power consumption of the transmitter.

The reflection-cancellation block is designed to have a timing resolution of one UI. This is often inadequate in removing complicated reflections that are generated by reactive loads. The current implementation of the reflection canceller is only capable of zeroing the reflection in the middle of the unit interval. To get better quality of reflection cancellation and a cleaner eye diagram, it is desirable to have a higher time resolution in the reflection canceller. The timing of each reflection-cancellation tap should have

a resolution of at least half of a unit interval so that reflections located in the interval boundaries are also cancelled.

Reflections often occur at multiple locations in the channel and they can be far apart from each other. The reflection canceller in this transmitter is limited to have only eight continuous taps. Thus, the reflection canceller cannot cancel multiple reflections that are separated by more than eight UIs. A more flexible tap assignment should be implemented such that the reflection canceller can cover a wider cancellation range.

The delay of the reflection-cancellation signals and the amount of compensation for each tap are parameters that require manual adjustment. This is inadequate for production chips. A receiver should be designed with a "back-channel" to send channel characteristics back to the transmitter so that these parameters can be automatically adjusted. The back-channel does not have to be a high-speed link since the operating environment of backplane systems changes slowly after operation. In the transmitter, circuits should be designed to take the information from the receiver and adjust the parameters accordingly.

The power consumption of the transmitter can be reduced by disabling the flip-flops that are not in the delay path of the variable delay block. By disabling the clock signals that drive these flip-flops, unnecessary switching activity is eliminated resulting in power saving.

References

[AM00]   P. Andreani and S. Mattisson. On the use of MOS varactors in RF VCO's. *JSSC*, 35(6):905–910, June 2000.

[Buc03]   A. Buchwald. Basics of serial backplane transceivers. ISSCC presentation, February 2003.

[DP97]   W. J. Dally and J. Poulton. Transmitter equalization for 4-Gbps signaling. *IEEE Micro*, page 48, 1997.

[FMWK97]   A. Fiedler, R. Mactaggart, J. Welch, and S. Krshnan. A 1.0625 Gbps transceiver with 2x-oversampling and transmit signal pre-emphasis. *IEEE International Solids-State Circuits Conference, Digest of Technical Papers*, pages 238–239, 1997.

[HHM00]   S. H. Hall, G. W. Hall, and J. A. McCall. *High-Speed Digital System Design, A Handbook of Interconnect Theory and Design Practices*. John Wiley and Sons, 2000.

[IEE93]   IEEE. IEEE standard test access port and boundary-scan architecture. *IEEE Standards*, October 1993.

[JM97]   D. Johns and K. Martins. *Analog Integrated Circuit Design*. John Wiley and Sons, 1997.

[KFM02]   Y. Kudoh, M. Fukaishi, and M. Mizuno. A 0.13-um CMOS 5-Gb/s 10-meter 28AWG cable transceiver with no-feedback-loop continue-time post-equalizer. *Symposium On VLSI Circuits Digest of Technical Papers*, page 64, 2002.

[LWJ03]   C-H Lin, C-H Wang, and S-J. Jou. 5Gbps serial link transmitter with pre-emphasis. *IEEE*, page 795, 2003.

[NSO99]   B. Nikolic, V. Stojanovic, and V. G. Oklondzja. Sense amplifier-based flip-flop. *IEEE International Solid-State Circuits Conference*, page 282, 1999.

[Rab96]   J. M. Rabaey. *Digital Integrated Circuits - A Design Perspective*. Prentice Hall, Inc., 1996.

[Raz01]   B. Razavi. *Design of Analog CMOS Integrated Circuits*. McGraw-Hill International Edition, 2001.

[Son96]   B-S. Song. NRZ timing recovery technique for band limited channels. *IEEE International Solid-State Circuits Conference*, pages 194–195, 1996.

[SR01]   J. Savoj and B. Razavi. A 10Gb/s CMOS clock and data recovery circuit with frequency detection. *IEEE International Solid-State Circuits Conference*, page 78, 2001.

[TTM+03]   H. Takauchi, H. Tamura, S. Matsubara, M. Kibune, Y. Doi, T. Chiba, H. Anbutsu, H. Yamaguchi, T. Mori, M. Takatsu, K. Gotoh, T. Sakai, and T. Yamamura. A CMOS multi-channel 10Gb/s transceiver. *IEEE International Solid-State Circuits Conference*, page 72, 2003.

[ZWS+03]   J. Zerbe, C. Werner, V. Stojanovic, F. Chen, J. Wei, D. Kim G.Tsang, W. Stonecypher, T. Thrush A. Ho, R. Kollipara, G-J. Yeh, M. Horowitz, and K. Donnelly. Equalization and clock recovery for a 2.5-10Gb/s 2-PAM/4-PAM backplane transceiver cell. *IEEE International Solid-State Circuits Conference*, page 80, 2003.